ELECTROCHEMICAL ETCHING OF SIC MATERIALS AND MODIFICATION OF PROPERTIES

ELECTROCHEMICAL ETCHING OF SIC MATERIALS AND MODIFICATION OF PROPERTIES

By

ZIMO JI, B.Eng.

A Thesis Submitted to the School of Graduate Studies in Partial Fulfilment of the Requirements

For the Degree

Master of Applied Science

McMaster University

MASTER OF APPLED SCIENCE (2025)

Hamilton, Ontario (Materials Science and Engineering)

TITLE: Electrochemical Etching of SiC Materials and Modification of Properties

AUTHOR: Zimo Ji, B.Eng. (Queen Mary University of London)

SUPERVISOR: Professor Adrian Kitai

NUMBER OF PAGES: xii, 96

Abstract

With the development of semiconductor physics and technology, the third-generation semiconductor, silicon carbide (SiC), has been developed for several decades, and a mature industry and market have been built up. For optoelectronic applications, SiC is an attractive material, because of its wide energy band gap. Due to the indirect band gap and high cost of fabrication, the real applications are not as good as III-V materials such as GaN. However, from the aspect of sustainability, the reservoir of group III elements such as Ga is quite limited, which cannot satisfy the increasing demand for products such as LEDs and displays. In this situation, SiC is in abundance and must play a significant role in the future.

This thesis focuses on the electrochemical etching strategy of SiC materials, exploring the effects of surface reconstruction and modification on their properties. In Chapter 4, a comprehensive study of electrochemical etching is provided by characterizing the surface with SEM, including the reaction mechanism, key parameters, and usage of different etchants with the relationships in between. Apart from that, a highly reflective porous structure was achieved by adjusting the etching parameters with dilute HF. The reflectivity was successfully explained by multilayer interference effects and shows the potential to be applied as optical reflectors and sensors. Besides, surface chemistry and size results were studied with XPS, Raman and XRD to provide a better understanding of the effects of etching.

In Chapter 5, a simple strategy for selective etching of patterns was proposed

assisted with surface scratching. The applied forces during scratching were explored with the ability to adjust the width of the pattern as observed by SEM and AFM. The formation mechanism is explained by the redistribution of electric field due to the amorphization, which is experimentally checked by TEM and theoretically verified by simulation modeling.

Acknowledgment

Time flies — two years have passed in the blink of an eye. Yet, at the same time, it moves slowly, with every moment bringing new thoughts, emotions, and experiences. So first and foremost, I want to express my gratitude: to life and time, to everyone I've encountered along the way, and to this imperfect yet endlessly fascinating world.

I am deeply grateful to my supervisor, Prof. Kitai, whose patience and encouragement have supported me throughout this journey. His profound knowledge and insight have been invaluable both within and beyond the scope of my research, constantly helping me grow and improve.

To my colleagues and classmates, thank you for your daily conversations and encouragement. Your diverse perspectives and suggestions have broadened my thinking and enriched my path.

To my friends, thank you for your companionship and presence in my life — you have made it all the more meaningful.

To my family, thank you for your unwavering support and respect. Because of you, I've had the confidence and peace of mind to pursue my passions and explore the world with conviction.

To everyone — thank you! May you all find peace with the past, joy in the present, and hope for the days to come.

Table of Contents

List of Figures

List of Tables

Table of Abbreviations

LED – light emitting diode

SBD - Schottky barrier diode

MOSFET - metal-oxide-semiconductor field-effect transistor

BJT - bipolar junction transistor

IGBT - insulated-gate bipolar transistor

MEMS - micro-electro-mechanical systems

UV – ultraviolet

PL – photoluminescence

CL - cathodoluminescence

QY - quantum yield

QD – quantum dot

SEM - scanning electron microscopy

TEM - transmission electron microscopy

EDS - energy dispersive spectroscopy

XRD - X-ray diffraction

AFM - atomic force microscopy

XPS - X-ray photoelectron spectroscopy

DBR - distributed Bragg reflector

FIB - focused-ion beam

Chapter 1

Introduction

1.1. Semiconductor Materials and Optoelectronics

Semiconductors are a group of materials with unique properties of electric conductivity between conductors (e.g., metals) and insulators, which have changed the world since they were first discovered in the 17th century.[1] Semiconductor materials widely exist on earth and can be classified as elemental semiconductors such as silicon (Si) and germanium (Ge) and compound semiconductors (e.g., II-VI and III-V compounds)[1]. With the development of two more centuries, the properties of semiconductors have been comprehensively explored, and a huge modern industrial sector has been built based on semiconductor materials and devices, from electrical components (e.g., transistors) to commercialized electronic products (e.g., computers and smartphones) as summarized in **Figure 1.1**. Until now, semiconductors are continuously undergoing research and development, from the synthesis of new materials (e.g., organic materials and quantum dots)[2][3] to the discovery and exploitation of properties and techniques (e.g., quantum computing and spintronics)[4][5].

Optoelectronics is one of the most typical applications of semiconductors, relying on the photoelectric effect discovered by Heinrich Hertz in 1887, which refers to the

interaction of light with materials and the conversion between light and electric signals. Optoelectronic devices, including light-emitting diodes (LEDs), photodetectors, and photovoltaics, not only delight the world but also play an indispensable role in various fields of human society, such as energy production, digital displays, and health care.

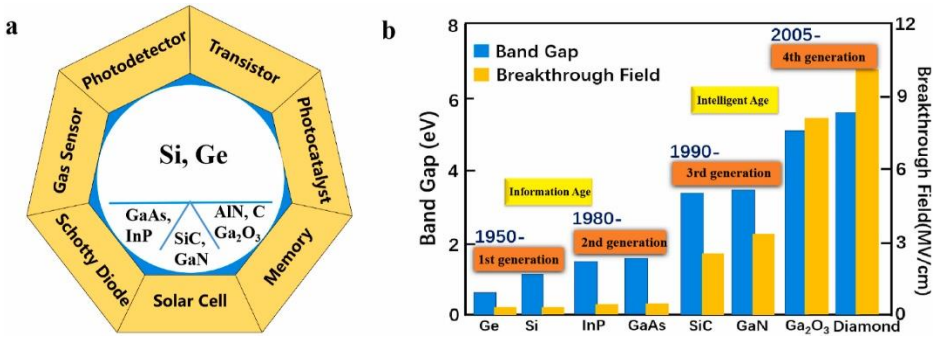

Figure 1. 1 (a) Classification and applications of semiconductor materials and (b) Progress of semiconductors with their band gap.[6]

1.2. Silicon Carbide Materials and Properties

Silicon Carbide (SiC) is a type of IV-IV compound material, which exhibits wide band gaps and is regarded as a third-generation semiconductor. The strong Si-C covalent bonds provide excellent mechanical and thermal properties. As one of the best-known examples of a material exhibiting polytypism, SiC has plenty of polytypes based on changes of stacking sequences, which can be normally classified into cubic, hexagonal, and rhombohedral. In industry, three typical crystallographies are discussed and utilized, including 3C (cubic site), 4H, and 6H (hexagonal sites) as shown in **Figure 1.2**.

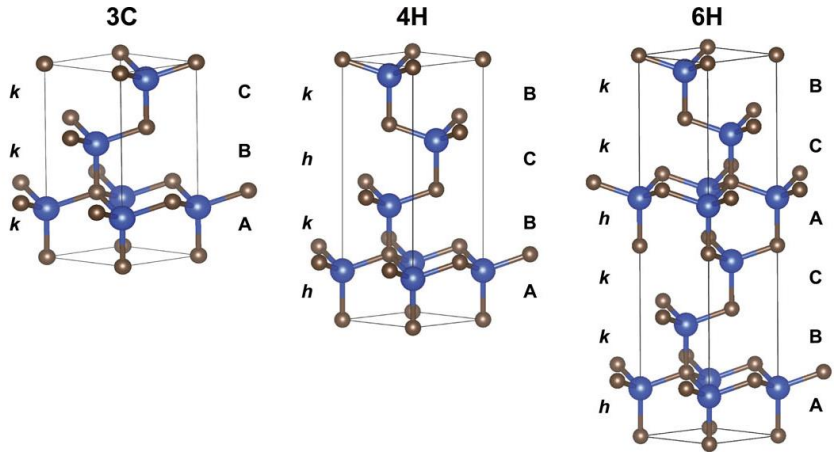

Figure 1. 2 Crystal structures of typical SiC polytypes including 3C, 4H and 6H[7].

For the materials properties, as mentioned strong Si-C bonds provide excellent mechanical properties of SiC materials, including bulk modulus, shear modulus, hardness and toughness[8], which make SiC an outstanding ceramic as a structural material. As a semiconductor, electric properties are more critical in terms of various applications. A summary of some key properties is presented in **Table 1**. One of the most essential differences among polytypes is the energy bandgap, which directly determines their usage. 3C-SiC has a narrow band gap, while 6H/4H-SiC provides a wider band gap and can be commercially applied in power electronics. Especially for optoelectronics, wide band gap materials are attracting more attention and interest due to their ability to generate or respond to deep blue or ultraviolet light[9]. Meanwhile, considering the carrier mobility, the high value and high uniformity of 4H-SiC make it more reliable.

Table 1. 1 Summary of electric properties of SiC between 3C, 6H and 4H[10][11]:

Properties		3C	6H	4H
Hexagonality		0	0.33	0.5
Lattice constant at 300 K (Å)	a direction	4.349	3.081	3.076
	c direction		15.079	10.05
Band gap at 300K (eV)		2.35	3.08	3.28
Breakdown electric field (MV/cm)		0.8	1	3
Saturate electric drift velocity (cm/s)		2.7×10^7	2×10^7	2×10^7
Thermal conductivity (W/cmK)		4.9	4.9	4.9
Hole mobility at N_A=$10^{16}\,cm^{-3}$ (cm^2/Vs)		10	90	115
Electron mobility at N_D=$10^{16}\,cm^{-3}$ (cm^2/Vs)		750	$\parallel c-axis$: 60 $\perp c-axis$: 400	$\parallel c-axis$: 800 $\perp c-axis$: 800

1.3. Silicon Carbide Fabrication Techniques

There has been a sophisticated technique and mature industry for fabricating SiC single crystal based on seeded sublimation growth (as shown in **Figure 1.3** below) developed by Lely in 1955 and improved by Tairov and Tsvetkov in 1978, which involves a process where SiC source material sublimes and recrystallizes on a seed

crystal under high temperatures. During the growing process, temperature control is very important directly affecting the polytypes of as-grown crystals.

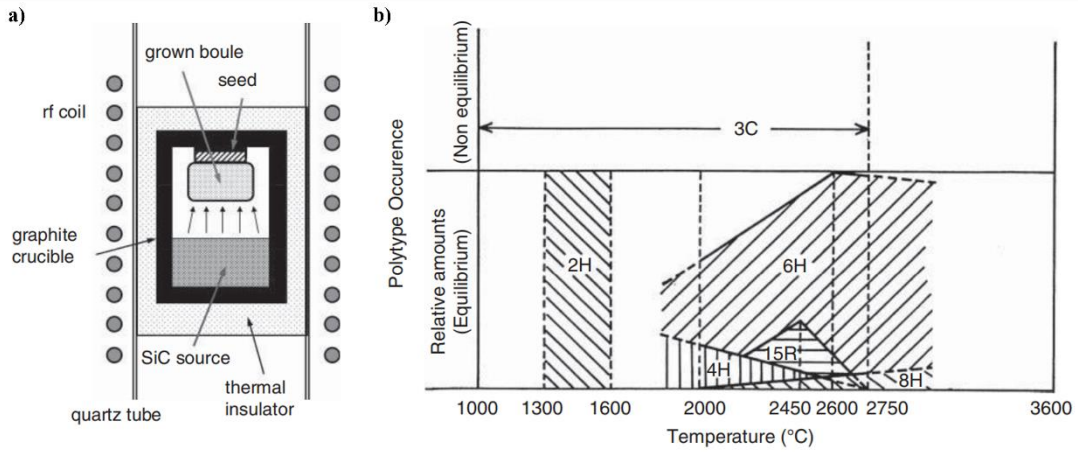

Figure 1. 3 (a) Illustration diagram of setups for seeded sublimation growth of SiC and (b) influence of temperature on the polytypes[12].

The inducing of defects is another challenge for industrial manufacturing of SiC considering the quality of as-grown SiC single crystals. Defects can be normally classified as bulk defects (3D), plane defects (2D), line defects (1D) and point defects (0D)[13]. The most widely existing defects are stacking faults (typical bulk defects) coming from the variation of polytypes[14]. To eliminate the formation of detrimental defects, many strategies have been proposed and developed continuously such as repeated a-face method[15]. Until now, SiC single crystals have been achieved for the 8-inch wafer industry and, the global market is expected to the grow continuously in the following decades.

1.4. Silicon Carbide-based Devices

Thanks to the high level of breakdown electric field and thermostability, SiC has been widely applied to power electronics so far commercially and has been developed with many structures of power electronic devices such as the Schottky barrier diode (SBD), the metal-oxide-semiconductor field-effect transistor (MOSFET), the bipolar junction transistor (BJT) and the insulated-gate bipolar transistor (IGBT) as illustrated by **Figure 1.4**. Even though there are some other competitive candidate materials such as silicon (Si) and gallium nitride (GaN), SiC shows remarkable reliability in high power applications compared with Si, and has relatively low prices with ideal long-term sustainability than GaN on account of natural resources.

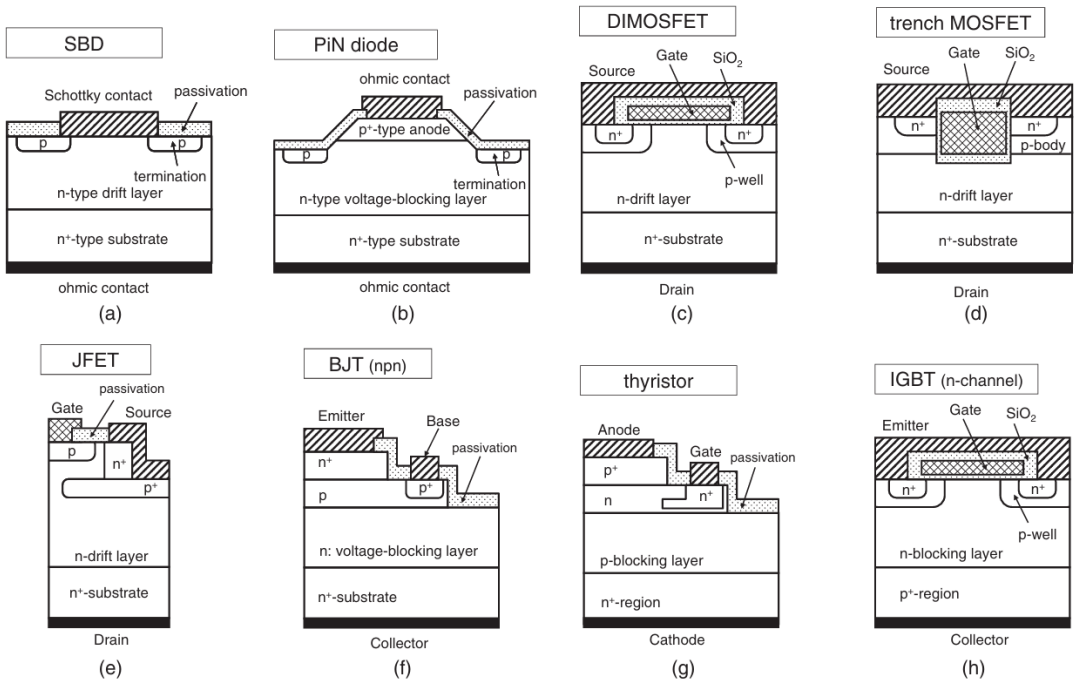

Figure 1. 4 Summary of well-developed structures for SiC power electronics.[16]

Beyond power applications, the properties of SiC also make it possible to be applied in a variety of applications. According to their mechanical strength and

chemical inertness, SiC has been considered in micro-electro-mechanical systems (MEMS)[17].

As for optoelectronics, the wide bandgap brings the ability for bandgap engineering to achieve specific applications. On the other hand, the indirect band gap makes it more suitable for photodetectors and photovoltaics considering the carrier mobility and lifetime.[18] For instance, the wide band gap of 4H-SiC shows its significance for ultraviolet (UV) photodetectors. In addition, certain point defects have recently been studied as color centers for single-photon emitters, playing an essential role in photonics and quantum sources[19]. When thinking about the interdisciplinary nature of SiC with bio-medical fields, SiC is one of the best candidates due to its excellent biocompatibility and bio-safety concerns compared to other well-known biomedical platforms such as gold and silver particles. Until now, SiC has attracted lots of interest in applications such as biosensors and bio-imaging.[20]

1.5. Challenges of Silicon Carbide

Even though SiC is famous for its remarkable properties and has achieved significant success in industry and technology, there are still some challenges that affect the future development of SiC materials and devices.

From the aspect of mechanical properties, it has two sides. On the one hand, the perfect mechanical strength makes it reliable as structural materials and brings potential, e.g., in MEMS. On the other hand, however, high thermal and chemical stability also

makes it very difficult to machine or fabricate into certain counterparts or precise micro/nanostructures to reach the requirements of certain devices and applications. For example, in the semiconductor manufacturing process, wet etching is one of the most commonly used approaches due to its high speed and low costs, which is favorable for large-scale production[21]. It refers to using some chemical such as acids and bases to react with the aimed materials directly. Nevertheless, SiC cannot be chemically etched as easily as other normal semiconductors such as Si and GaN because of its chemical stability even under extreme conditions (e.g., high temperatures or hazardous hydrofluoric acid (HF) environments)[22]. In this scenario, SiC materials have to be fabricated by dry etching, for which materials are exposed to bombardment of ions (e.g., plasma of gas). Although it has some advantages such as perfect control of etching precision, the cost is still relatively high, so it is still not the first preference compared to simple wet etching. To overcome this challenge, several strategies were proposed, including electrochemical etching and metal-assisted chemical etching.

Based on electronic properties, the indirect band gap limits the applications in LEDs, suffering from the low efficiency, compared to another mature commercialized material, GaN, due to the requirement of phonons in excitation and recombination processes[23]. With research and development in recent years, SiC has been shown to have fluorescent properties relying on surface defects or quantum confinement[24]. The photoluminescence (PL) quantum yield (QY) has been successfully improved up to 60% for SiC quantum dots (QDs)[25]. This progress brings attention back to SiC and

provides the possibility for industrial applications in the future.

1.6. Research Objectives

The objective of this thesis is to modify the structures of porous SiC by electrochemical etching approach and achieve special microstructures for photonic applications such as optical reflectors, which includes the study of the electrochemical etching mechanism, the influence of etching parameters, and their effect on surface morphology and properties. Meanwhile, the selective etching effect is also proposed by inducing defects to broaden the potential applications of electrochemical etching techniques.

Chapter 2

Theoretical Background

2.1. Semiconductors Physics

2.1.1. Band Theory

Band theory is a theoretical model in solid-state physics describing the behavior of electrons in solids related to other particles (e.g., atoms), and it is the basis of semiconductor physics. In crystals with periodic systems, electrons are arranged as energy bands due to the interactions of particles (e.g., electron-electron, electron-atoms). To simplify the wavefunction in Schrödinger equation, Bloch functions and König-Penney model make contributions to define the wavefunction of electrons and potentials in a periodic solid system. Based on the interpretation of near-free electrons and the tightly binding approximation, the formation of energy bands can be defined by the splitting of atomic energy levels in solids with periodic potential as shown in **Figure 2.1(a)**. From the bonding theory, when two electrons from two different atoms form a chemical bond, it can further split into allowed and forbidden bands separately as shown in **Figure 2.1(b)**, according to the formation of bonding and anti-bonding energy states from the linear combination of electrons' wavefunctions. Overall, based on the value of the energy band gap, all the materials can be classified into conductors, insulators and semiconductors.

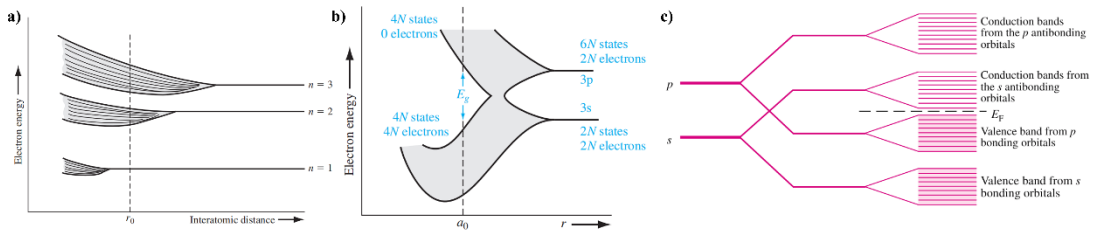

Figure 2. 1 Illustration diagram of splitting of energy states (a) with tightly binding model and (b) bonding model[1]; (c) Formation of energy bands by overlapping of bonding and anti-bonding energy states[26].

2.1.2. Direct & Indirect Band Gap

During the interpretation of energy band structures, the statements of electrons and atoms for their positions and relationships are discussed in reciprocal spaces (k-space), which emerged from Fourier transformation of crystal lattices and is directly used for the derivation of electronic properties. According to the k space of band structures, semiconductors can be divided into direct and indirect band gaps, depending on whether the minimum of conduction band and the maximum of valence band have the same momentum or not (as shown in **Figure 2.2**).

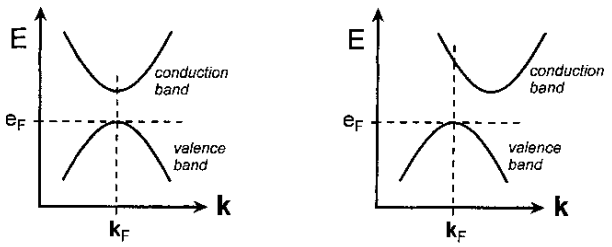

Figure 2. 2 Illustration of band structures for direct and indirect semiconductors.[27]

2.1.3. Excitation & Recombination

When the materials are excited by external energy (e.g., photon, thermal energy,

etc.), electrons will be activated from the ground energy state to a higher energy state, which is defined as the excitation process in semiconductors where electrons are able to be excited from valence band into conduction band. At the same time, holes are also generated in valence band. Once the electrons are activated to excited states, which are not stable, they will relax back to the stable ground states. In semiconductors, excited electrons changing from conduction band back to the valence band is defined as the recombination process. Depending on the different behavior of electrons, the recombination process can also be divided into band-edge recombination, defect recombination, and Auger recombination as shown in **Figure 2.3**. In general, band-edge recombination is called radiative recombination because the energy loss is dominated by emission of a photon, while all the other recombination processes are often regarded as non-radiative recombination which have the negative effect of lowering the quantum efficiency. But these processes still play an essential role in certain kinds of applications.

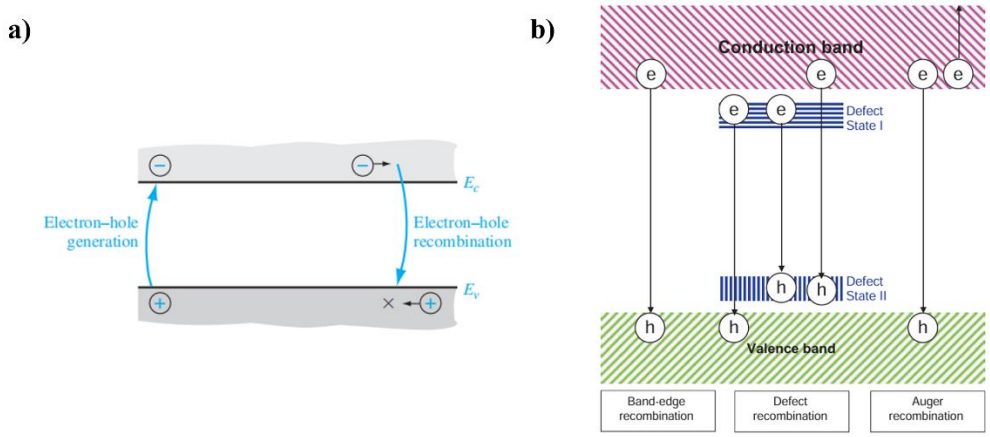

Figure 2. 3 (a) Illustration of excitation and recombination processes[1] and (b) Different types of recombination processes in semiconductors[28].

2.1.4. Photon & Phonon

Both photon and phonon belong to the class of boson particles, which follow the explanation and statistics in quantum mechanics, and exhibit wave-particle duality[29]. Correspondingly, photon refers to a particle of light bearing energy, while phonon is represented as a quantum of vibrational energy in solids.

In semiconductors, both particles are incorporated in excitation and recombination processes as shown in **Figure 2.4**. In general, photons can react with semiconductor materials, in which materials will first absorb the photon to excite electrons and holes (excitation process), then the electrons will relax to valence band again (recombination process) with emission of a photon. This light-material interaction is defined as an example of the photoelectric effect, which is the basis of optoelectronic materials. When discussing the direct band gap, it just follows the process mentioned above. For the indirect band gap, however, it requires changing the momentum of electrons and has to incorporate phonons in both excitation and recombination processes. This phonon-assisted two-particle behavior suffers from a low probability in quantum physics, leading to a low quantum efficiency for LED applications[30].

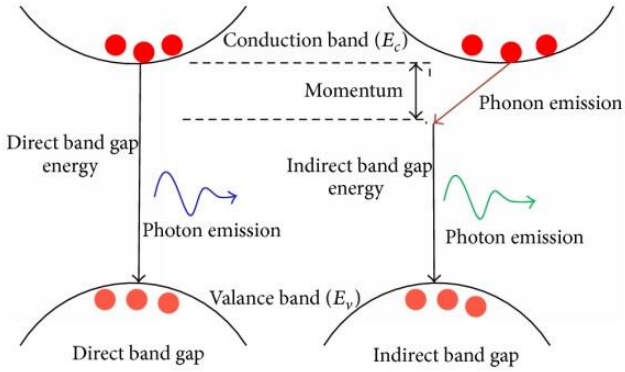

Figure 2. 4 Role of photons and phonons in direct and indirect band gap semiconductors.[31]

2.1.5. Doping Engineering

Doping is one of the key technologies in semiconductor band gap engineering, which refers to adding additional elements from adjacent groups. In definition, pure semiconductors are named as intrinsic semiconductors while doped semiconductors are named as extrinsic semiconductors. Specifically, dopants can be classified as donors and acceptors, depending on their role to provide extra electrons or holes based on the number of valence electrons. Donors will create a donor energy level lower than the minimum of conduction band (called n-type), while acceptors will form an acceptor energy level above the maximum of valence band (called p-type), it will affect the electric properties, for example changing photon energy due to the doping energy levels (as shown in **Figure 2.5**). For doping techniques, doping elements can be added during the sublimation growth or deposition processes, which are direct and useful for large scale production[32]. Otherwise, it could also be achieved after crystal growth by

implantation, which allows better control including the selective doping areas, change of doping types and concentration[33]. This is unique for the fabrication of a variety of devices with P-N junctions.

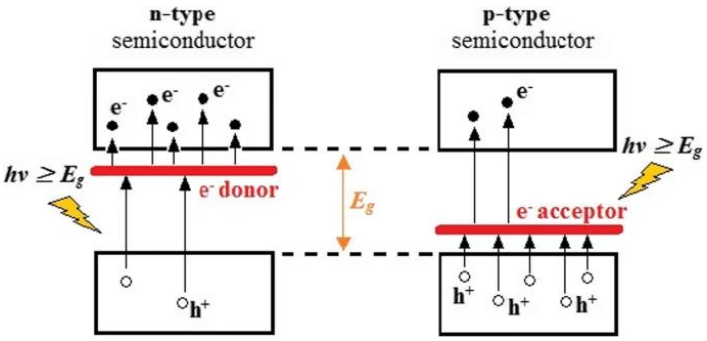

Figure 2. 5 Band diagram illustration of n-type and p-type semiconductors by doping.[34]

2.1.6. P-N Junctions and Devices Operation

P-N junctions are the basis of semiconductor devices, which combine both n-type and p-type semiconductors and have critical electric properties at the interface (shown in **Figure 2.6**). First, the carriers (electrons and holes) will diffuse to another part due to the gradient of carrier concentrations. At the same time, once the carriers diffuse, a built-in electric field will form at the interface of junctions. This electric field will force the carriers to move as well (called drift), in the opposite direction of diffusion. There is a balance between diffusion and drifting, and it will eventually reach an equilibrium where the drifting force equals the diffusion force. In this equilibrium state, no free carriers are moving between the junction, where the region is defined as the depletion region.

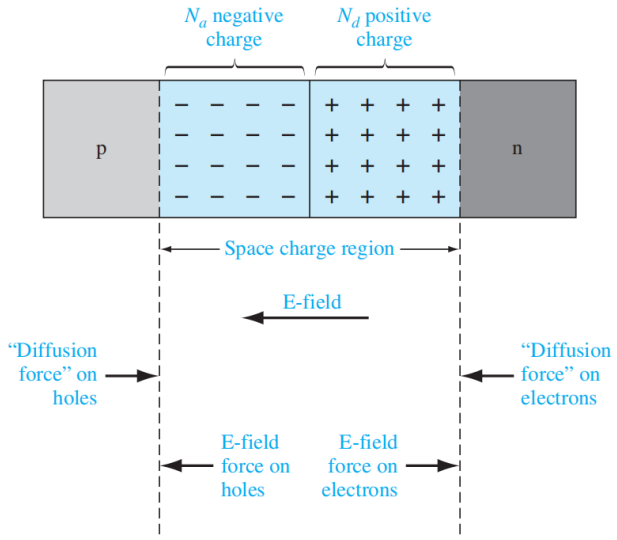

Figure 2. 6 Model of P-N junction and carriers' behavior.[1]

For the operation of P-N junctions and devices, an external voltage will be applied, which will break the equilibrium and make the net charge non-zero. When the P side is connected to the positive terminal (called forward bias), the external electric field has the opposite effect on the built-in electric field, leading to carrier transport in the direction of diffusion and giving a thinner depletion region. Inversely, if the P side connects to the negative terminal (called reverse bias), it will enhance the built-in electric field and enlarge the depletion region[35]. Both forward and reverse modes play significant roles in different devices.

2.1.7. Quantum Confinement Effect

With the requirement for sizes of devices and the development of fabrication techniques, materials can be fabricated with smaller sizes (e.g., in nanometer scale) or

in lower dimensions (e.g., 2-dimensional materials or 0-dimensional quantum dots). During the reduction of material sizes, it is found that the electric properties change dramatically. In terms of physical scale for quantum mechanics, the special electron behaviors can be explained by the quantization of energy, where the energy level tends to be discrete compared to classical continuous ones (illustrated in **Figure 2.7**). This effect of crystal sizes or dimensions is defined as quantum confinement effects.

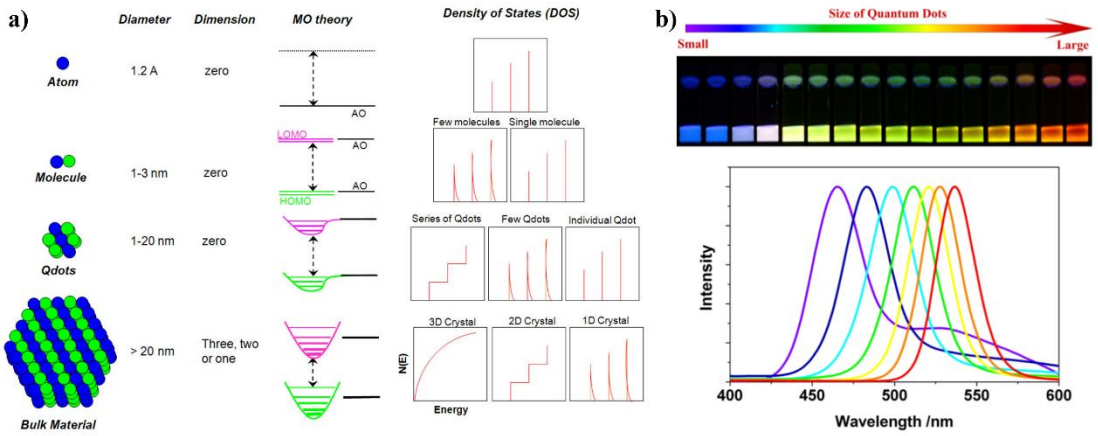

Figure 2. 7 (a) Effect of quantum confinement on energy level and density of states; (b) Effect of crystal size on the band gap and corresponding light emissions.[36]

2.1.8. Defects & Color Centers

Defects exist widely in almost all materials, inevitably due to many reasons, including the originally existing defects in raw materials, defects formed during crystal growth, defects generated by post-treatment, and defects produced in the operation of devices[37]. For example, as mentioned in the section on SiC fabrication above, there

are multiple types of defects likely to form during the sublimation growth.

Generally, for electronics, defects are regarded as detrimental issues that negatively affect the stability and performance of devices. However, defects also bring some unique properties. Based on the theoretical calculation and experimental observations, their energy levels are located within the energy band gap of semiconductors (as shown in **Figure 2.8** for SiC), and play an interesting role during excitation and recombination processes such as fluorescence emitted from defects. For instance, O-related defects in ZnO have been shown with the ability to emit greenish light and have been commercially applied in industry such as the vacuum fluorescent display of microwave ovens and other appliances[38]. For SiC, defects also receive much attention due to their potential not only in optoelectronics to generate fluorescence, but also their ability as single photon emitters from defect color centers, which is very useful in quantum computing[39].

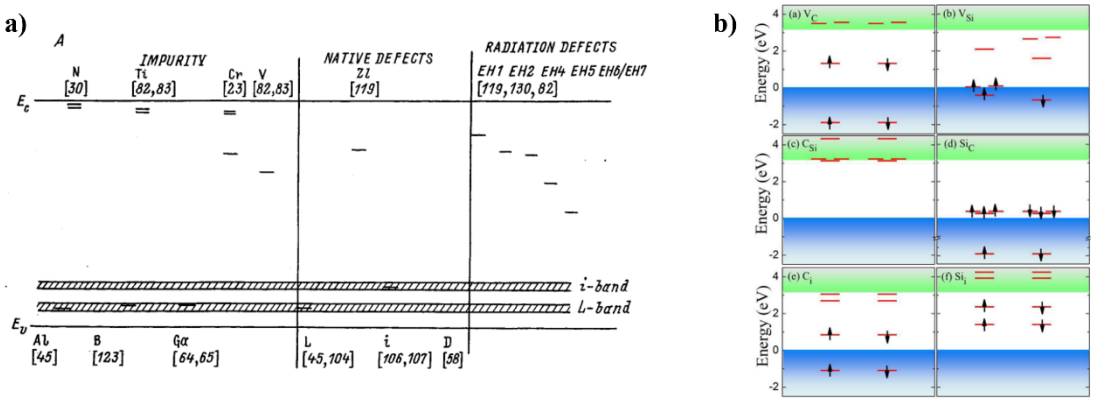

Figure 2. 8 Summary of (a) deep-level defect centers [40] and (b) point defect centers [41] in the band diagram of SiC.

2.2. Wet Etching Techniques

2.2.1 Chemical Etching

The conventional wet etching, or “chemical etching”, is to directly etch the semiconductors with liquid chemicals such as acids or bases. According to the chemical activity of different semiconductors, and recipes also change with different chemicals, mechanisms and final effects. For example, for group IV semiconductors (e.g., Si and Ge), the etching process comprises first oxidation and then further reaction to transform the solid-state semiconductors into other dissolvable species. The etchants should include an oxidizing agent (e.g., HNO_3 or H_2O_2) and reactive agent (e.g., F^- or OH^-), where the commonly used etchant for the Si industry is HNO_3 plus HF[42]. For III-V semiconductors, not limited to the previous mechanism, some chemicals can directly react with them to form some soluble species. For example, hydrochloric acid (HCl) can react with indium phosphate (InP) to form InCl in solution and PH_3 gas[43]. Depending on the requirements of etching effects, for example isotropy or anisotropy, appropriate etching solutions should be selected with precise control of etching rate and resolution. Even though the precision of wet chemical etching is not as ideal as dry etching, the simple setups and the low cost for both money and time make it dominant in large-scale production.

However, this conventional approach suffers from the problem of low etching rate even when operating at an elevated temperature. Also, it is almost impossible to treat some chemical materials (e.g., SiC). In this scenario, some new etching strategies have been emerging in recent years.

2.2.2 Photo-assisted Chemical Etching

In the basic chemical etching, the oxidation process is only driven by the chemical potential of the oxidizing agent. Only if the redox potential is higher than the potential of semiconductors, the valence electrons of semiconductors will be depleted in further oxidation reactions. This this case, the etching rate is highly dependent on the energy level of semiconductors and the redox potential agents, which is limited due to the selection of oxidizers. From chemistry aspects, it has been reported that electrons and holes have unique properties as well for reduction and oxidation[44]. Based on that, if semiconductors are excited by photons with energy higher than their band gaps, there will be photo-generated electrons and holes in the conduction band and valence band correspondingly, where the holes could assist the oxidation reaction to improve the etching rate (as shown in **Figure 2.9**).

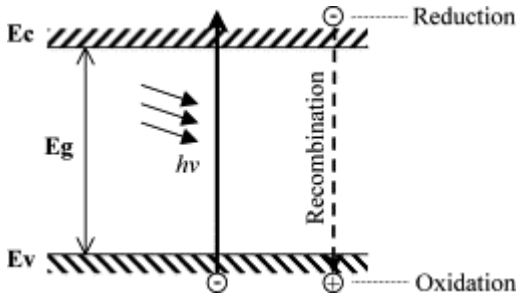

Figure 2. 9 Illustration of the mechanism for photo-assisted etching[22].

2.2.3 Metal-assisted Chemical Etching

Metal nanoparticles play an important role as catalysts, resulting from their high surface areas and electrical properties.[45] In wet etching processes, metal particles can

also work as catalysts to improve the etching effects. By using similar content of etchant solutions, including oxidizer and reactive ions, the deposited metal on the surface of semiconductors could work as electrodes, where cathodic reductions will happen to reduce the oxidizer by losing electrons. During this process, since the electrons of metal are obtained by oxidizers, there will be plenty of holes on the surface of metal, able to transport into the semiconductor substrates. As discussed in the previous section holes have oxidation properties; thus, there will be further oxidation reactions of semiconductors (regarded as 'anodic reactions')[46]. The oxidized semiconductor will then react with certain ions (e.g., HF) persistently with an enhanced etching effect (as shown by the example in **Figure 2.10(a)**). Similarly to the requirement of chemical potential for oxidizing agents in conventional chemical etching, the potential of metals compared with the energy level of semiconductors also determines their catalytic abilities in metal-assisted etching (as shown by an example of Si in **Figure 2.10(b)**), the appropriate metal catalysts should be selected for various semiconductors[47].

On the other hand, combining the photo-assisted etching, it will have a different effect on metal-assisted etching, where the holes can be transported to the surrounding regions and give an inverse effect as shown in **Figure 2.10(c)** (named as inverse metal-assisted etching)[48]. The challenge of this approach comes from the selection of metals with appropriate chemical potential. For SiC, it has limited options, and Pt is always required for the etching process which is costly. Meanwhile, it brings some difficulties in fabrications such as the deposition of arranged metal particles and their removal

afterward.

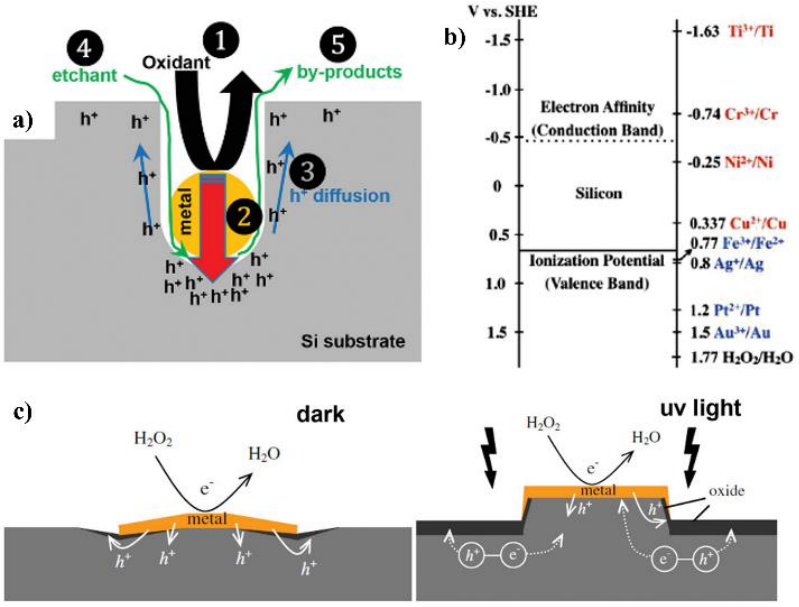

Figure 2. 10 (a) Mechanism of metal-assisted chemical etching; (b) Summary of appropriate metal catalysts for Si; and (c) Illustration of inverse effect of etching.[49]

2.2.4 Electrochemical Etching

Electrochemical etching refers to applying voltages on semiconductors, and conducting and accumulating electrons and holes for the enhancement of etching rate. This method no longer needs high temperature or special metal catalysts but only requires the materials or devices to be conductive and able to connect in circuits as demonstrated in **Figure 2.11(a)**. The role of applied voltage is to build an electric field and accumulate sufficient holes for oxidation reactions, especially for p-type semiconductors with enough holes. However, for n-type semiconductors, donors only provide extra electrons instead of holes. In this case, photo-assisted etching is also combined to generate sufficient holes continuously during etching[50]. Considering the

difference between conventional chemical etching and electrochemical etching, the surface morphologies achieved are slightly different as exhibited in **Figure 2.11(b)-(c)**. Since the built electric field is the dominant factor in electrochemical etching, and the distribution of the electric field can be affected by the structures of various dielectric materials, electrochemical etching tends to form porous structures based on the preferential accumulation of holes[51].

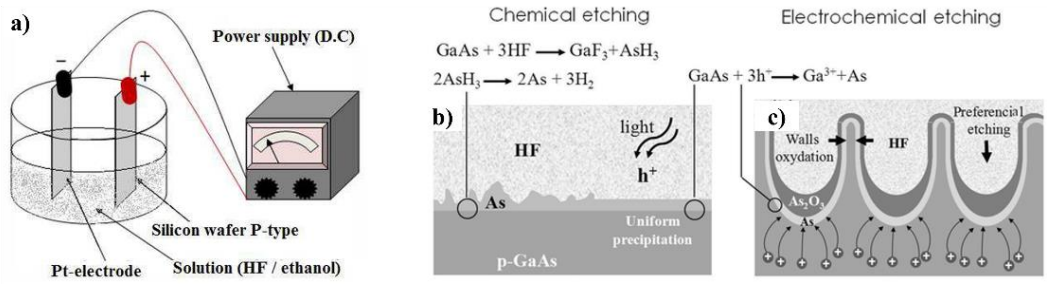

Figure 2. 11 (a) Illustration of electrochemical etching system[52]; Comparison of carrier transportation and etching effect for (b) chemical and (c) electrochemical etching[53].

Chapter 3

Materials & Characterization Methods

3.1. Materials Preparation

3.1.1. Raw Materials

To conduct the research project on SiC materials, a single crystal n-type (10^{18} cm^{-3} nitrogen-doped) 4H-SiC wafer (4-inch) with a thickness of 350 μm was purchased from MSE Supplies LLC and diced into 1 cm × 1 cm dies. Specifically, both the Si-face [0001] and C-face $[000\bar{1}]$ of the wafer were subjected to chemical mechanical polishing, achieving a surface roughness of Ra 0.5 nm. Additionally, the wafer was fabricated with a 4-degree miscut toward the $[11\bar{2}0]$ direction by the manufacturer.

3.1.2. RCA cleaning

The SiC dies were cleaned by the standard RCA process[54] every time before experiments. Initially, the die underwent ultrasonic cleaning in acetone, methanol, and propanol, each for a duration of 5 minutes. This was followed by a multi-step chemical cleaning protocol. The first step involved immersion in a 1:1 volumetric mixture of concentrated sulfuric acid (98%) and hydrogen peroxide (30%) for 15 minutes. Subsequently, the die was treated in a 1:1 solution of ammonia (98%) and hydrogen peroxide (30%) at 80 °C for 15 minutes. The final chemical cleaning stage consisted of

immersion in a mixture of hydrochloric acid (37%), hydrogen peroxide (30%), and deionized water in a 1.5:1.5:5 volume ratio at 80 °C for 15 minutes, aimed at removing residual organic compounds and ionic impurities. Each chemical treatment step was followed by rinsing with 10% HF and deionized water. The wafers were then dried under a nitrogen gas stream.

3.1.3. Sputtering of Ni Electrode

To connect the SiC die to the circuit for further electrochemical etching, a thin film of nickel (Ni) was deposited on the C face of SiC by magnetron sputtering. Once the SiC die was cleaned, it was loaded into the sputtering chamber. Then the Ni electrode was sputtered using an Angstrom Science ONYX-02IC Standard Magnetron sputtering gun fitted with a Ni sputtering target (purchased from ChangSha XinKang Advanced Materials) with a 50.8 mm diameter and 0.5 mm thickness. During the sputtering process, the basic pressure was first pumped lower than 5×10^{-6} Torr to remove potential contaminations. Then the deposition was held at 100 W sputtering power and 10 mTorr sputtering pressure for 90 s in the argon environment at room temperature.

3.2. Electrochemical Etching Cell

To set up the electrochemical etching, an etching cell was constructed manually. The specifications of the designed etching cell are shown in **Figure 3.1**. The main body was made by a Teflon rod which is chemically stable in HF solution. Inside the rod, a

hollow structure was drilled as the container of etchant. At the bottom of the rod, a small hole was made which is the contact area of solutions and SiC dies, where the size was determined to be a bit smaller than the size of SiC dies. To seal the setup and prevent leakage, a groove was also made outside the contacting hole, and an O-ring was put there to seal between the Teflon and the die. Last, additional holes were drilled for screws to fasten the counterparts between the top rod and the substrate disk. During the etching operation, the target surface (Si face) was put upward and exposed to the etchant, while the backside did not contact the corrosive solution to protect the Ni electrode and guarantee the connection of the electric circuits. Meanwhile, a platinum (Pt) bar was applied as a cathode by connecting to the negative terminal, while the SiC was connected to the positive terminal as an anode. Since the purchased SiC is n-type, an additional 365 nm UV lamp was applied on top to generate holes during the etching process.

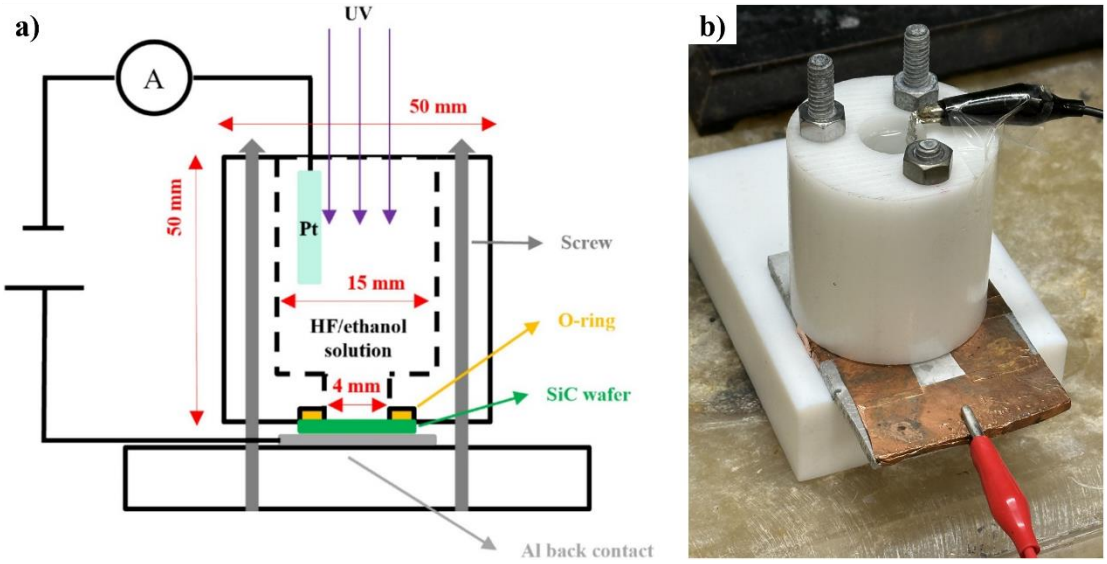

Figure 3. 1 (a) Structure of electrochemical etching cell [55] and (b) a photograph.

3.3. Characterization Techniques

3.3.1. Scanning Electron Microscopy (SEM)

Scanning Electron Microscopy (SEM) coupled with Energy Dispersive Spectroscopy (EDS) was employed to examine the surface morphology and verify the elemental composition of the materials. SEM analyzes materials by detecting secondary electrons generated through the interaction between the incident electron beam and the sample surface. These interactions produce various signals, including secondary electrons, backscattered electrons, and characteristic X-rays (as summarized in **Figure 3.2**). Surface morphological features are primarily revealed through secondary electron imaging, where variations in surface angle lead to contrast differences in the resulting image. EDS, commonly integrated with SEM, is utilized for compositional analysis. In this technique, the detector captures the characteristic X-rays emitted as a result of the electron beam interacting with the sample atoms. The elemental composition is then determined based on Moseley's law, which correlates the frequency of emitted X-rays with the atomic number of the elements present.

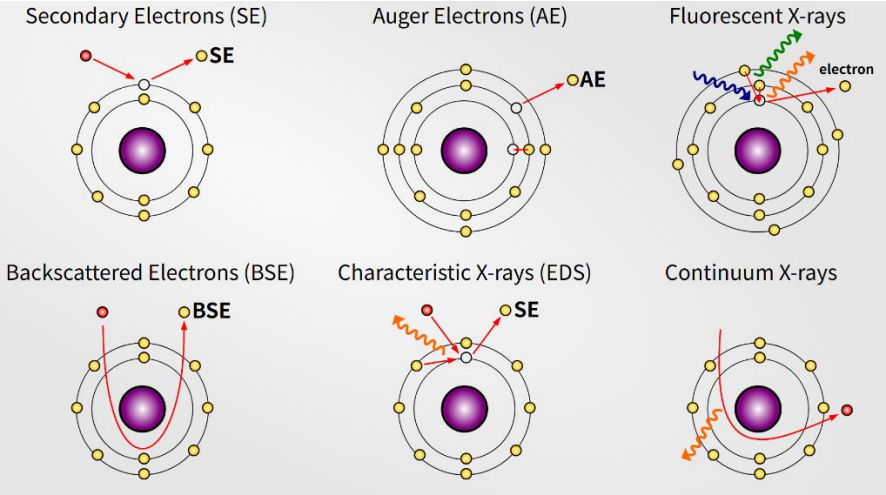

Figure 3. 2 Summary of interactions between the electron beam and materials.[56]

In this research, all the SEM facilities are provided by Canadian Centre for Electron Microscopy (CCEM) including an FEI Magellan 400 high-resolution SEM and a Thermo Scientific Quattro environmental SEM.

3.3.2. Transmission Electron Microscopy (TEM)

Transmission Electron Microscopy (TEM) is extensively employed in scientific research owing to its ultrahigh resolution, which enables detailed analysis at the atomic scale. This technique requires the preparation of ultra-thin specimens to allow electron beam transmission through the sample. When coupled with Energy Dispersive Spectroscopy (EDS), TEM provides a comprehensive characterization of materials, including detailed information on crystal structures, lattice parameters, dislocation features, and high-resolution spatial imaging of the crystalline architecture and chemical compositions.

In this research, the sample preparation and characterization of TEM was also assisted by CCEM using a Thermo Scientific Talos 200X.

3.3.3. X-ray Diffraction (XRD)

X-ray diffraction (XRD) is a widely utilized and well-established technique for the characterization of materials and the identification of crystal structures. When X-rays interact with a material, diffraction occurs based on Bragg's Law (shown in **Figure 3.3**), enabling the analysis of both crystalline and, to some extent, amorphous phases. Due to its versatility and reliability, XRD is among the most frequently employed methods in materials research. Beyond general phase identification, XRD is also extensively applied in texture analysis, structural determination, estimation of microcrystalline size, and the evaluation of both macro and micro-level residual stresses. Its broad range of applications makes it an essential tool in the study of material microstructures.

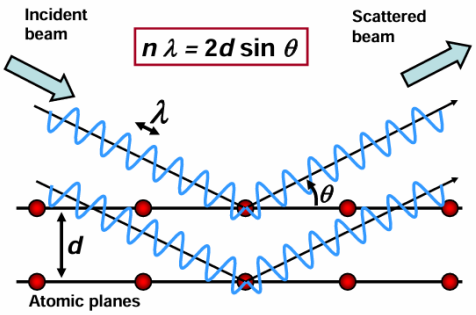

Figure 3. 3 Principle of XRD measurement based on Bragg's Law.[57]

In this research, XRD characterization was operated in McMaster Analytical X-Ray Diffraction Facility (MAX) on a Burke D8 Venture machine.

3.3.4. Raman Spectroscopy

Raman spectroscopy is used to identify the vibration of materials based on the inelastic scattering of crystals. In the scattering theory, when light interacts with materials, it is defined as elastic scattering (or Raley scattering) if the energy of incident light does not change, which often occurs for small particles. However, a large number of materials exhibit another phenomenon, in which the energy of light changes after interacting with materials due to the inelastic scattering of crystals or molecules. In principle, electrons will be excited into a higher energy state, however, they may not follow the same pathway when coming back. In most cases, the energy will get lost due to the relaxation process by vibration, which is named Stokes scattering and the lost energy is called Stokes shift. While in some cases, the energy might increase which is called an anti-Stokes shift[58]. The shifted energy is used to analyze the vibration mode of materials and further identify the materials. Up till now, some developments have been made, such as surface-enhanced resonance Raman spectroscopy, to effectively increase the sensitivity of measurements (as summarized in **Figure 3.4**)[59].

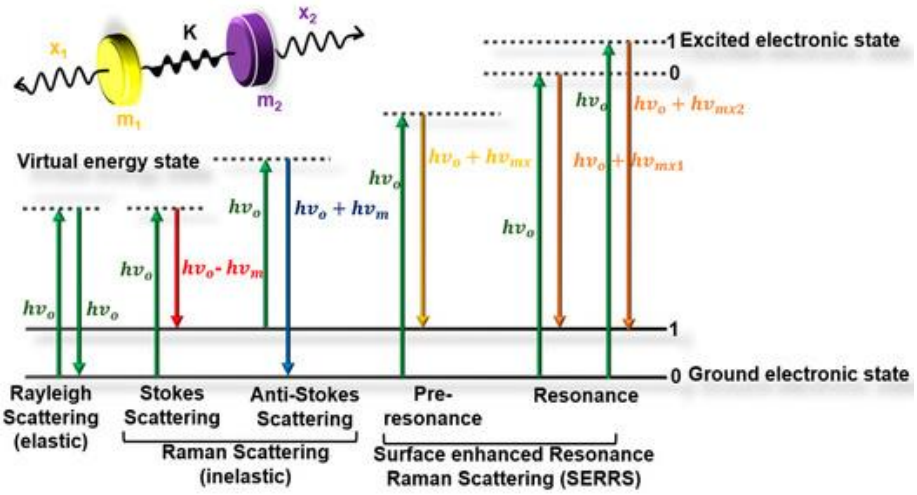

Figure 3. 4 Principle of light scattering and summary of different Raman techniques.[60]

In this research, the Raman spectroscopy is assisted by Prof. Alex Adronov's research group at Brockhouse Institute for Materials Research (BIMR) on an InVia confocal Raman microscope.

3.3.5. Confocal Microscopy

Compared to the conventional optical microscope, the confocal microscope can focus on a very tiny volume/thickness of the sample and selectively collect the fluorescent signal from aimed regions using a dichroic mirror and a pinhole, which could block the out-of-focus light. Not only can it improve the resolution in the Z-axis for capturing 3D images, but also the combined excitation and detection system could help to observe the surfaces and structures of fluorescent materials.

In this research, the confocal microscopy is assisted by McMaster Center of

Advanced Microscopy (CALM) on a Zeiss LSM 980 Inverted Spectral Confocal Microscope.

3.3.6. Atomic Force Microscopy (AFM)

Atomic force microscopy (AFM) is a type of probing technique with ultra-high resolution of surface topography, which is very helpful for the characterization of surface structures such as electronic devices[61]. For the working principle, the surface morphology is touched by a cantilever, and the information is detected and collected with a laser system where the reflected light records the height of the cantilever.

In this research, the AFM is used to measure the surface morphology of etched samples, which is also assisted by CALM on a Bruker Dimension iCon AFM.

3.3.7. X-Ray Photoelectron Spectroscopy (XPS)

X-Ray Photoelectron Spectroscopy (XPS) is used to characterize the surface chemistry, where the captured signal is from ultra-surface regions of materials thinner than a few nanometers and it could provide quantitative analysis such as for chemical positions and chemical states (e.g., chemical bonds). By this principle, the binding energy of core electrons to keep in their orbitals is the key characteristic, which is measured by photoionization of core electrons by irradiation with X-ray photons (as illustrated in **Figure 3.5**). The core electrons will eject from the materials' surface when they are ionized by a certain energy of X-ray photons.

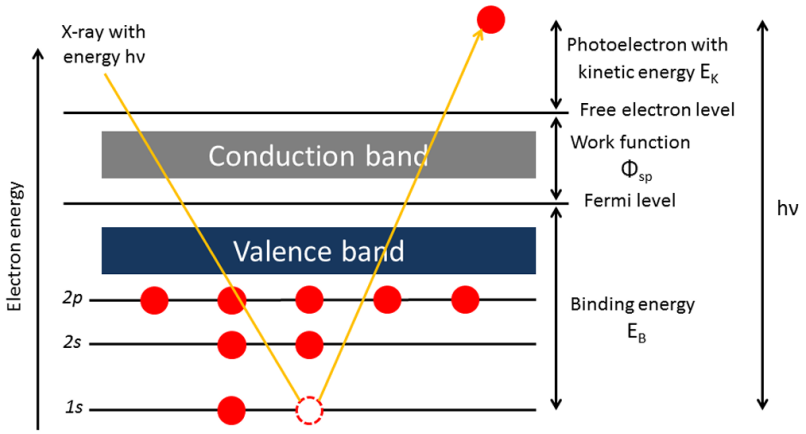

Figure 3. 5 Principle of XPS characterization.[62]

In this research, the XPS facility is provided and supported by McMaster Biointerfaces Institute (BI) based on a PHI Quantera II XPS spectrometer.

3.3.8. Photoluminescence & Cathodoluminescence

Photoluminescence (PL) and cathodoluminescence (CL) refer to the light emission properties by absorbing energy from photons (PL) or cathode rays (CL). For the light emission process, the electrons will first absorb the energy and be excited into conduction band, then during the recombination, it will emit a photon with energy correlated to the energy band gap of semiconductors. These two techniques are very useful to observe the fluorescent properties of materials. Meanwhile, they can both combine with microscopes (e,g, PL in an optical microscope system, CL in an SEM system) to observe materials in high resolution with more details of microstructures.

In this research, the PL measurement setup is provided by the research group of

Prof. Peter Mascher in McMaster Centre for Emerging Device Technologies (CEDT) with a 375 nm HeNe laser source from OBIS and UV–Vis spectrometer from Ocean Optics. The CL facility is provided by CCEM with a detector from Delmic inserted within Thermo Scientific Quattro ESEM.

3.3.9. Absorbance & Reflectance

When light interacts with materials, it has several optical phenomena (as concluded in **Figure 3.6**) including: 1) reflection at the surface, 2) transmission through the material, and 3) scattering or absorption inside the material. To describe the optical properties of materials based on these phenomena, some terms are defined such as absorbance and reflectance. Absorbance demonstrates the amount of light absorbed by materials, by calculating the logarithm of the ratio of incident to transmitted light intensity through the material[63] :

$$A = log_{10}(\frac{I_0}{I_{trans}}) \tag{3.1}$$

Absorbance is one of the effective strategies to measure the energy band gap of materials indirectly via drawing a Tauc plot from the absorbance spectrum. The reflectance refers to the amount of light reappearing at the surface after diffuse reflection, which can be calculated by the ratio of reflected to incident light intensity:

$$\rho_\lambda = \frac{I_{ref}}{I_0} \tag{3.2}$$

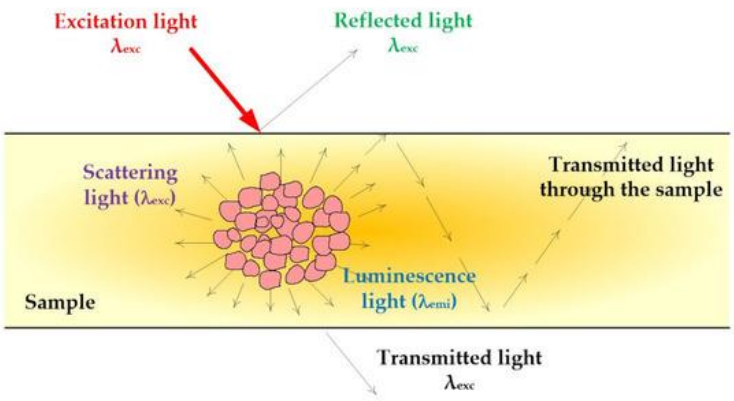

Figure 3. 6 Interactions of light and materials.[64]

In this research, the absorbance is measured by a Tecan Infinite M1000 PRO plate reader provided by McMaster Biointerface Institute (BI), while the reflectance measurement is assisted by Prof. Alex Adronov's research group on a Cary 5000 UV-Vis-NIR spectrophotometer.

Chapter 4

Porous Structures Achieved by Electrochemical Etching

4.1 Introduction

Porous semiconductors have been widely studied due to their critical microstructures and special effects on optical properties[65]. On the one hand, the porous materials have an ultrahigh surface area, which is favorable for surface engineering such as the highly sensitive sensors[66], or creates more active space to make composite devices by loading with other materials such as quantum dots-embedded porous GaN for micro-LEDs[67]. On the other hand, the porous structure itself brings interesting effects on the optical properties coming from both quantum confinement effects and surface defects color centers as discussed in Chapter 1. This remarkable phenomenon has been widely observed and studied in porous Si and Ge with strong photoluminescence[68][69]. Recently, SiC has also been reported with an enhanced PL based on electrochemically etched porous structures[70][71].

Porous SiC is commonly achieved through electrochemical etching due to its excellent chemical stability as discussed in Chapter 1. By controlling the etching conditions, various surface structures have been achieved with their unique properties. For example, Lu et al. had combined the porous SiC with another donor-acceptor co-doped SiC substrate to achieve white light emission[72], Wang et al had applied

electrochemically etching SiC nanowires to fabricate the ultra-sensitive UV detectors[73], and Rashid et al. reported the availability of electrochemical etching to prepare the fluorescent SiC quantum dots[74].

In general, the surface engineering of SiC is still under research and development, and in this chapter, a comprehensive study of electrochemical etching was conducted to further understand the effects of each parameter, and the new critical structure is achieved with ultrahigh optical reflectivity, which contributes to broadening the potential applications of SiC materials.

4.2 Experimental Details

4.2.1 Electrochemical etching

In this part of research, different parameters were applied and studied with their effect on the electrochemical etching of SiC. In specific, different etching solutions were utilized including HF and KOH aqueous solutions with various concentrations. Meanwhile, different values of current density were controlled during etching. Afterward, a certain parameter is used, based on the deep understanding of each parameter, to fabricate a highly reflective surface.

4.2.2 Characterizations of achieved structures

The surface morphology of etched samples was directly observed by SEM, and the elemental compositions were verified by EDS. The etching rate is observed by both

cross-sectional view of SEM and the AlphaStep profilometer. The surface chemistry was analyzed by XPS to obtain a deeper understanding of surface chemical reactions during etching. The optical properties of prepared samples were further measured by PL, CL and reflectance separately.

4.3 Results and Discussion

4.3.1 Electrochemical etching with KOH solution

According to the mechanism of electrochemical etching, SiC will be firstly oxidized on the surface with the assistance of holes:

$$SiC + h^+ + H_2O \rightarrow SiO_2 + CO_x + H^+ \quad (4.1)$$

The formed SiO_2 is a special oxide, which is resisted by most acids unlike other normal oxides. The etching of SiO_2 has been well developed in industry by HF aqueous solutions since Si-O bonds can be broken by HF due to the strong electron affinity of F[75]. Therefore, by electrochemical etching with HF solution, the following reaction will the decomposition of SiO_2 into dissolvable SiF_6^{2-}:

$$SiO_2 + HF \rightarrow {SiF_6}^{2-} + H_2O + H^+ \quad (4.2)$$

According to the literature review, molten alkanes such as KOH have been widely used to etch or polish the SiC surfaces based on the reaction with both Si-C bonds and oxidized Si-O bonds[76]. Similarly, KOH might also be available in electrochemical etching due to its ability to react with SiO_2, and the supposed reaction should be:

$$SiO_2 + OH^- \rightarrow {SiO_3}^{2-} + H_2O \quad (4.3)$$

At the preliminary stage of the experiment, KOH was chosen as the beginning on account of the safety issue considering the risks of HF. By adjusting the etching cell and circuit connections, the electrochemical etching is successfully achieved using our self-manufactured setup (as shown in **Figure 4.1**). For the etching parameter of this sample, 10 wt% KOH aqueous solution was used as the etchant, and the current density was controlled as 20 mA/cm^2 for a duration of 2 h. On the top surface, the circular black region is the etched part, where the black color is given by the change of surface morphology affecting the scattering/reflection of light. The multiple dark squares on the back side are the sputtered Ni contact electrodes, which also survived after etching, proving that the sealing of etching cell is also acceptable.

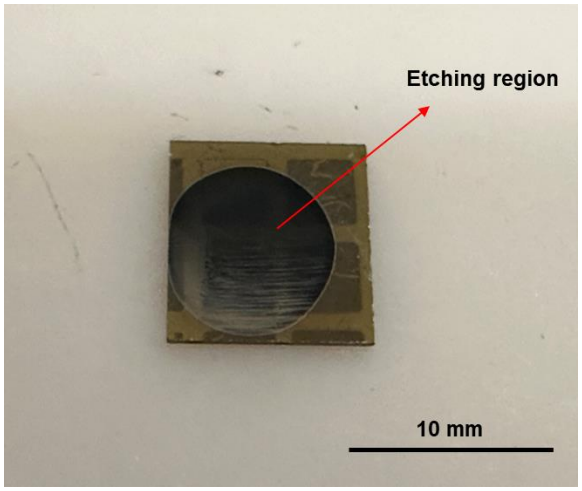

Figure 4. 1 Photograph of SiC die after electrochemical etching with KOH.

The surface morphology given by SEM also proves the formation of porous structures as shown in **Figure 4.2**. Combined with morphology and supposed etching reactions, the surface structure can be explained reasonably. The surface should be

firstly oxidized and further reacted by KOH at the same time. Since the oxides may not form uniformly, the initial oxide clusters will be immediately reacted to form some pores shown in **Figure 4.2(c)**, while some parts of the surface have not been fully oxidized or have been oxidized by not reacted yet, leading to some incompletely etched regions shown in **Figure 4.2 (b)**.

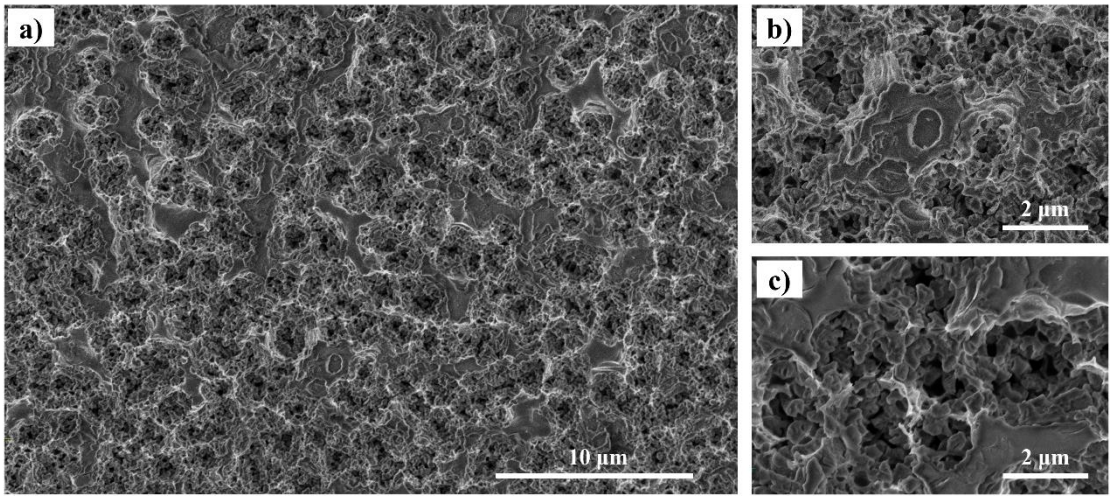

Figure 4. 2 (a) Surface morphology of sample etched with 10 wt% KOH solution with zoom-in images in high magnification for (b) incomplete etched region and (c) deep pores.

Due to the non-uniform surface of the previous sample, the etching parameter should be adjusted to improve the etching effects. Therefore, another sample was prepared by etching with 30 wt% KOH solution while other parameters were kept the same. Compared with the sample etched by 10 wt% KOH, this sample has a more uniform porous surface as shown in **Figure 4.3**. By observing zoom-in images, this sample has more tiny and homogeneous pores compared to the irregular surface of the previous sample. Meanwhile, the pore sizes of this sample are much smaller than the

previous one, which is all smaller than 1 micron (around 300-500 nm), this is more feasible for further development and application such as quantum confinement effects. The difference could be explained by the rate of two-step reactions. With the low concentration of KOH, the reaction of oxides is much slower and leaves a large area of incomplete etched region. While higher concentrations of KOH can react to the oxides more efficiently. Once the oxides are formed, they will be immediately etched by KOH, giving smaller pores.

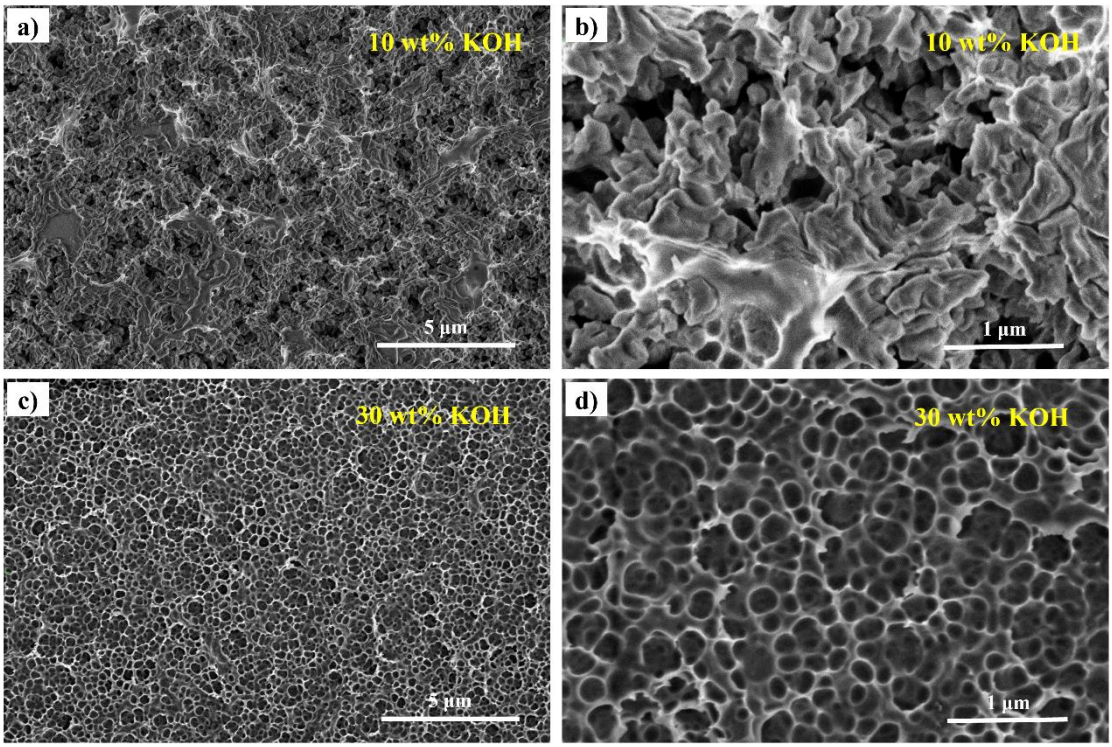

Figure 4. 3 Comparison of surface morphologies for (a) sample etched by 10 wt% KOH with (b) zoom-in image; and (c) sample etched by 30 wt% KOH with (d) zoom-in image.

In the etching process, one of the important things is the etching rate. To explore the etching rate, the sample was cleaved for cross-sectional SEM as shown in **Figure**

4.4. There are some inevitable cracks formed during cleavage. The high-mag image demonstrates the depth of the porous layer of about 500 nm (the dark rectangular is the damage due to the electron beam). Therefore, the etching rate of porous layer can be calculated at around 4.16 nm/min, which is extremely slow.

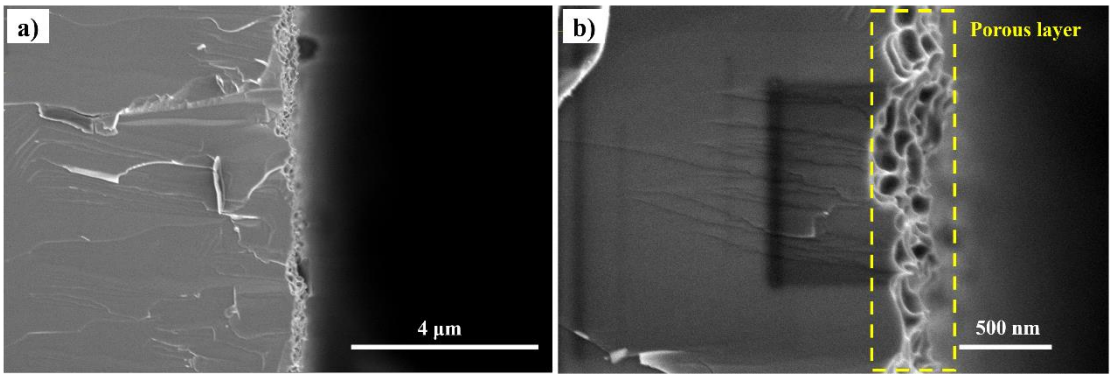

Figure 4. 4 Cross-sectional view of sample etched by 30 wt% KOH in (a) low magnification and (b) high magnification.

Now the KOH has been shown with the ability for electrochemical etching of porous SiC with relatively small pores. However, the low etching rate is one of the biggest limitations. According to the literature review, the porous SiC should be observed with an enhanced PL given by surface defects or quantum confinements. However, the KOH etched samples do not show the observable PL spectrum, which could be because the formed porous layer is too thin. The KOH is available to achieve some surface modifications but is not an effective way to produce bulk properties such as fluorescence. In this scenario, the HF-based etching solution is still necessary to study further.

4.3.2 Effect of concentration and current density with HF solution

Because of the limitations of KOH discussed in the previous section, a comprehensive study of etching with HF will be discussed in this section. Similarly, the effect of concentration was studied for HF as well. At the same time, based on the mechanism, the holes in semiconductors play a key role in the oxidation process, while the photo-generated holes should accumulate at the surface along the electric field provided by the applied voltage. The values of applied voltage (or current density equivalently) were also explored with their effects on etching.

To conduct the experiments, three different samples were prepared with different etching parameters as listed in **Table 4.1**. Specifically, a comparison of samples A and B can indicate the effects of current density, while a comparison of samples B and C can indicate the influence of HF concentration. The etching solution is mixed with the mentioned HF aqueous solution with ethanol in a volume ratio of 2:1 to improve the wettability of solutions, where ethanol is commonly used in the etching process as the surfactant[77]. The etching time was kept at 1 hour, and a 365 nm mercury lamp was applied as the UV light source.

Table 4. 1 Selected etching parameters for various samples:

	HF concentration	Current density (mA/cm^2)	Etching Time
Sample A	10%	80	1 h

Sample B	10%	20	1 h
Sample C	48%	20	1 h

SEM observations of three samples are shown **in Figure 4.5**. The main differences are the size of pores and the thickness of remaining SiC structures, where both the pore size and structure thickness increase from sample A to sample C. Compared with samples A and B, a higher current density tends to form more tiny pores and thin structures when using the same concentration of HF. Compared with samples B and C, a lower concentration of HF also achieves smaller pore size and thickness relatively. Back to the etching mechanism, the higher current density gives more accumulation of holes to speed up the first oxidation process, while the lower HF concentration reduces the reaction rate with as-formed SiO_2 in the second step. As a consequence, the surface morphology is highly dependent on the balance between two steps of chemical reactions – the first oxidation reaction and the second HF reaction.

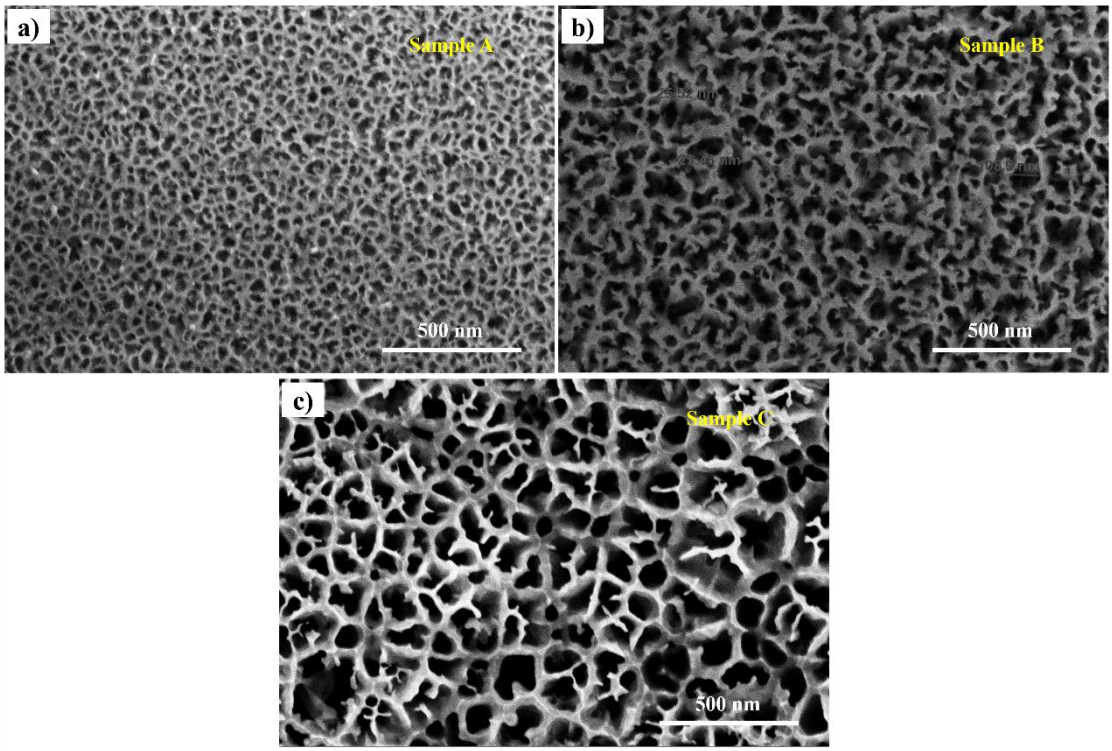

Figure 4. 5 Surface morphologies of (a) sample A, (b) sample B, and (c) sample C.

According to the investigation of the etching process, the formation of surface structures can be approximately explained by a simplified model shown in **Figure 4.6**. At the beginning, the holes will uniformly distribute near the surface to initiate surface oxidation. Once some oxide clusters form, they will be decomposed by HF in the meantime to form some preliminary pits. In the next stage, the holes are still moving to the surface driven by the applied voltage, but are more likely to accumulate at the bottom of the pits due to the enhanced field distribution. Under this behavior, surface oxidation tends to continue inside of holes to make the etched pits larger and deeper rather than form new pits on the top surface. During a period of time, the holes grow deeper and deeper, which brings more difficulties in transporting holes to the top surface,

and the diffusion of HF inside the hole also becomes harder. Eventually, the typical porous structures are achieved with various sizes of holes and thicknesses of remaining SiC materials. Combined with the etching parameters, higher current density could help to push more holes to the top surface, which eventually provides dense holes with smaller size and thickness. On the other hand, increasing the concentration of HF can improve the reaction rate with oxides, which tend to enlarge the holes and play an opposite role with the current density to some extent.

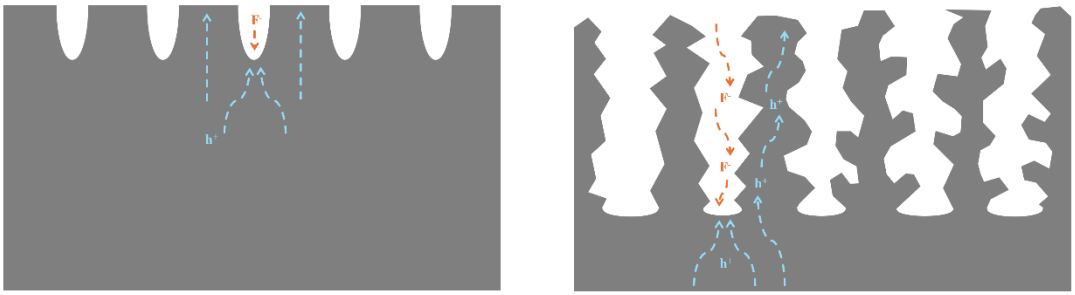

Figure 4. 6 Formation mechanism of porous structures based on the distribution of holes and F ions.

Similarly, the etching rate of various parameters was measured and summarized in **Table 4.2** as a reference for future work. Even though the low value of both current density and HF concentration gives the weakest etching effects, there is not a clear trend due to the complexity of the dynamics of two chemical reactions and real structures.

Table 4. 2 Measurement of etching rate with different etching parameters:

	HF Concentration	Current density	Etching rate

		(mA/cm^2)	
Sample 1	5%	20	1.3 μm/min
Sample 2	10%	20	0.47 μm/min
Sample 3	2%	20	0.53 μm/min
Sample 4	5%	2	66 nm/min
Sample 5	48%	20	1.1 μm/min

4.3.3 Formation of highly reflective structures

During the verification of various etching parameters, it was found that there is a lack of information about using dilute HF solutions based on the literature review. The commercial products of HF aqueous solution are 48%, and most of the reported usage is greater than 10%. However, according to the discussion above, the surface morphology is highly dependent on the balance of two key parameters – current density and HF concentration. To explore the unknown conditions, some samples were prepared under the dilute HF solution, and some interesting results were found.

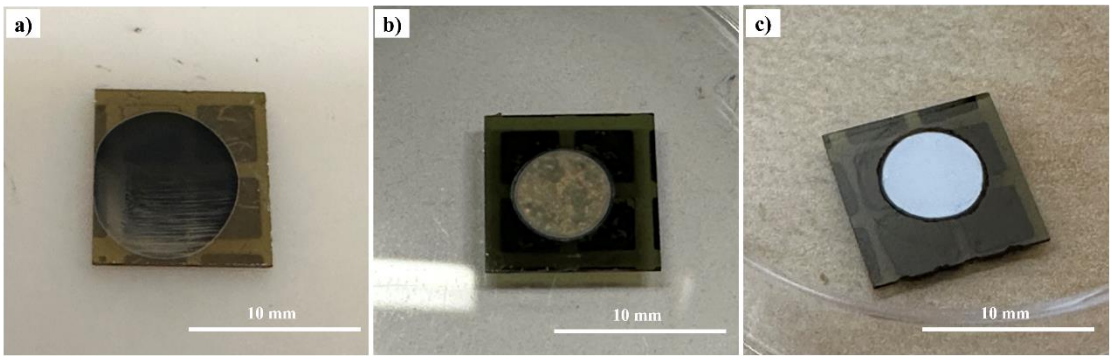

Figure 4. 7 Photographs showing the surface appearance of samples etched by different solutions: (a) by 10% KOH, (b) by 10% HF, and (c) by 5% HF with the same

current density of 20 mA/cm^2.

As shown in **Figure 4.7**, there are different colors for samples prepared in different conditions. Normally, porous surfaces or powder-like surfaces will exhibit a dark appearance such as black, grayish, or brown due to the increase of surface roughness and enhanced surface scattering from the irregular surfaces[78][79]. However, etching with dilute HF showed a bright white appearance, which is rare in SiC materials. In order to fully understand this phenomenon, more characterizations were done including SEM-EDS observation, XPS for surface chemistry, XRD and Raman for materials identification.

First of all, to eliminate the possibility of any contaminations or impurities during the preparation, SEM-EDS was applied to check the chemical composition of the white sample. As the results are shown in **Figure 4.8**, the white surface is almost made by Si and C with a bit of O, which demonstrates that the sample is still pure SiC with some inevitable surface oxidation.

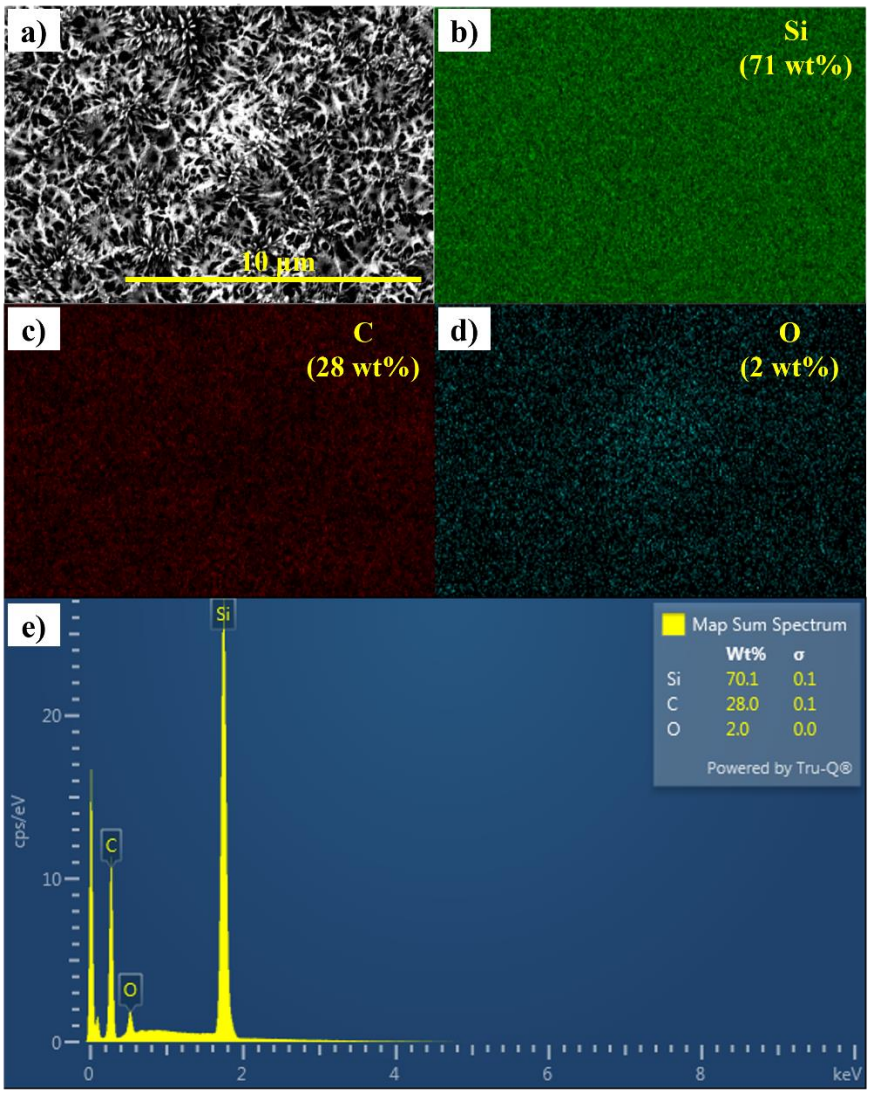

Figure 4. 8 SEM-EDS analysis: (a) morphology mapped region, (b)-(d) mapping analysis for Si, C, O element, and (e) spectrum.**Error! Bookmark not defined.**

By excluding the irrelevant factors, the change should be only given by the reconstruction of the surface after etching. Since there is not any dye molecule and SiC does not have white fluorescent under room light, its whitish surface should be a structural color, which is caused by the reflection of visible light[80]. In principle, materials can reflect light in a certain range of wavelengths due to their microstructures,

which can be observed by eyes and defined as structural color. In our case, the white color is a bit special since white light is a mixing of all visible light (such as red, green and blue in commercial LEDs), which means that the achieved surfaces are able to reflect almost all the visible light, working as an excellent light reflector. To verify the suspect, the reflectance spectrum was measured to directly find out the relationship between reflectivity and wavelength (as shown in **Figure 4.9**). According to the results, the white sample has an ultrahigh reflectivity and is even higher than 90% in most of the visible light range. Compared with that, the pristine SiC only has very low reflectivity (that is reasonable since the wafer is semi-transparent). With this consequence, it can be concluded that the white color comes from the reflection of visible light.

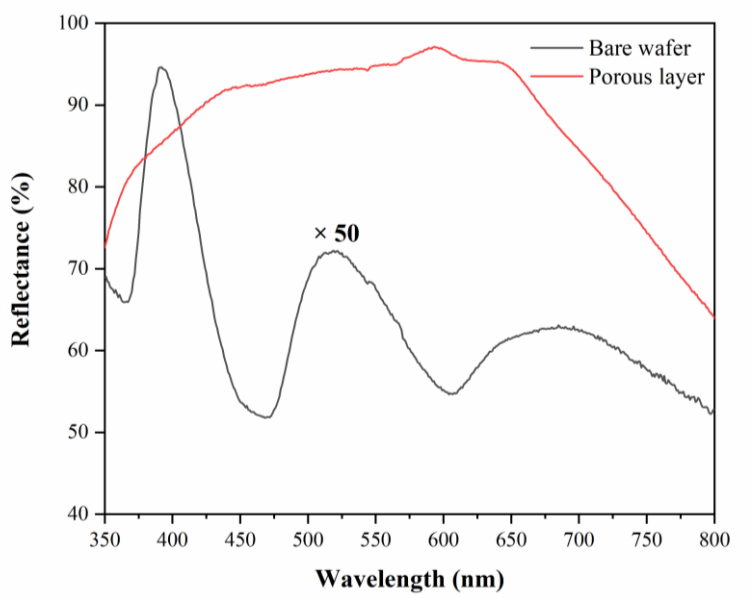

Figure 4. 9 Reflectance spectra of the white porous sample compared to a pristine wafer.[55]

To build a connection between as-measured high reflectivity with the surface structures, high-resolution SEM was used to observe both surface and cross-sections (as shown in **Figure 4.10**). From the top view of surface morphology, it can be observed that the etched surface is not like any normal porous structures as shown and reported before but has lots of distinctive flower-like structures. Based on the image in high magnification, it is clear that the 'flowers' are made by plenty of free-standing needle-shape structures, and the size of these nano-needles is mostly smaller than 100 nm. In this scale, these free-standing nano-needles have quantum confinement effects, similarly to nanowires, exhibiting the potential for many applications such as field emissions[81][82]. Even though it has a distinctive surface structure, it still cannot explain the high reflectivity. To further understand the structures, cross-section SEM was done by cleaving the sample to form a clear edge. The cross-section view shows that the sample has a special layered structure with plenty of branches stacking with each other. Considering the alternative SiC layers and air gaps, the reflectivity can be thus understood by the constructive interference of multiple reflections from the materials with different refractive indices, which is defined as the multilayer interference effect[83].

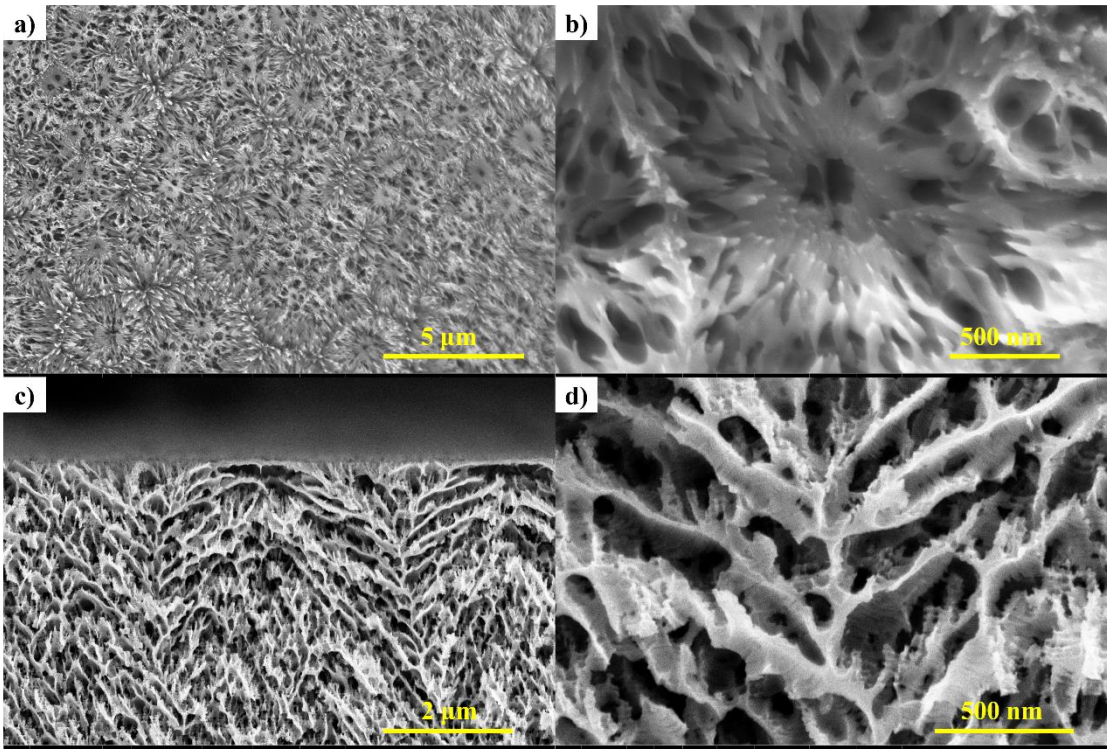

Figure 4. 10 SEM images of the white porous sample with (a) - (b) top views, and (c) - (d) cross-sectional views.**Error! Bookmark not defined.**

To understand the multilayer interference effects in our sample, a theoretical study was conducted by constructing a model. According to the literature review, one of the most popular models relying on multilayer interference effects is the distributed Bragg reflector (DBR), consisting of two alternating layers with different refractive indexes[84]. According to the theory of wave interference, constructive interference of reflected light occurs when the phase difference arising from variations in optical path length between adjacent layers corresponds to half the wavelength of the incident light. This condition results in a significant enhancement of reflectivity. In this model, the phase difference is determined by the product of the refractive index and the physical

thickness of the interlayer, representing the effective optical thickness of the material. Based on the observed structure from cross-section SEM, a simplified model was made as presented in **Figure 4.11(a)**, in which a pair of SiC and air layers are alternating. Correspondingly, the reflectivity can be calculated by:

$$R = \left(\frac{1-\left(\frac{n_H}{n_L}\right)^{2N}\frac{n_H^2}{n_a n_s}}{1+\left(\frac{n_H}{n_L}\right)^{2N}\frac{n_H^2}{n_a n_s}}\right)^2 \quad (4.4)$$

Here, n_H and n_L denote the refractive indices of the two alternating dielectric layers, while n_a and n_s represent the refractive indices of the external medium (air) and the substrate, respectively. The parameter N indicates the number of repeated bilayer units. In this configuration, the thicknesses of the SiC and air layers were set to 50 nm and 125 nm, respectively, based on experimental observations. The refractive indices were assigned as 2.64 for SiC and 1.00 for air.

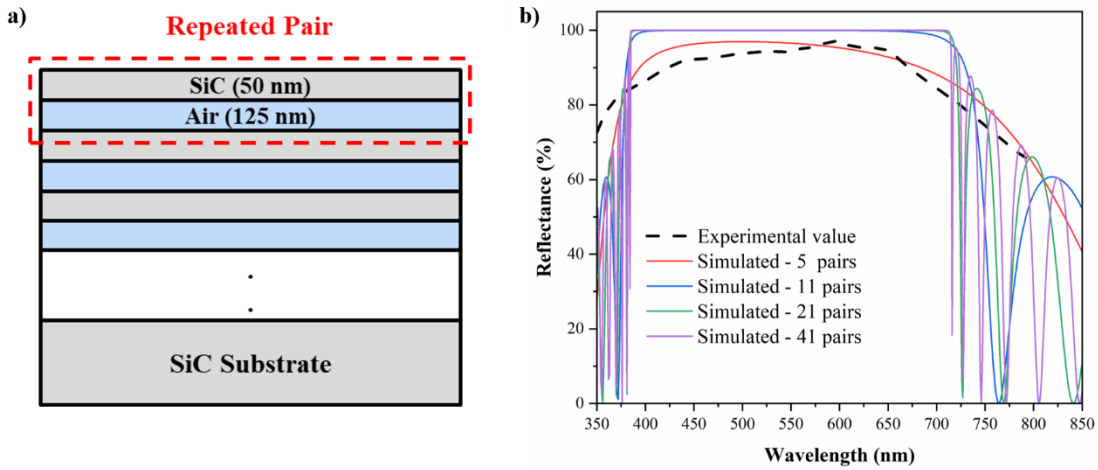

Figure 4. 11 (a) Constructed model in simulation and (b) Comparison of simulated and experimental results of reflectance.[55]

The simulation outcomes are presented in **Figure 4.11(b)**. The experimentally

measured reflectance (represented by the dashed line) closely follows the overall shape and trend of the simulated spectrum corresponding to five pairs (indicated by the red line). This resemblance can be attributed to the limited penetration of light into the deeper layers of the structure. The observed deviation between the experimental data and the simulated results for five pairs is justifiable, given the non-ideal nature of the actual structure. In practice, the fabricated material exhibits greater structural complexity, including variations in layer thickness, slightly inclined surfaces, numerous free-standing nanoneedles, and unavoidable surface terminations and oxidation. These factors collectively influence the optical response, particularly the reflection and refraction behavior. Although the distributed Bragg reflector (DBR) model cannot fully capture the exact reflectance characteristics of the real sample, the close correlation between simulation and experiment strongly supports the interpretation that the high reflectivity originates from the formation of a reasonably ordered layered nanostructure through electrochemical etching.

To date, highly reflective SiC structures of this nature have not been previously documented; instead, prior studies have primarily reported the anti-reflective characteristics of SiC[85]. Owing to the exceptional thermal stability of SiC, the demonstrated multilayer configuration holds promise for applications in high-temperature environments, including aerospace systems[86]. On the other hand, compared with typical DBRs, this structure is much easier to fabricate with one-step electrochemical etching. Otherwise, a number of thin films should be grown or

deposited layer by layer, which increases the cost and consumes plenty of time. Furthermore, the porous structures generated through etching present an opportunity for chemical detection and sensing. When exposed to various chemical species that can be adsorbed within the multilayer architecture, these materials may exhibit distinct spectral or color changes, some of which could be visible to the naked eye, offering a promising approach for visual or spectroscopic sensing applications. To achieve better control of reflected wavelengths, further research is needed to tune the thickness of SiC and air layers.

Apart from structures, some other characterizations were also done to give a comprehensive analysis of this sample including surface chemistry, size effects, and fluorescent properties.

The surface bonding configurations were investigated through X-ray photoelectron spectroscopy (XPS) to gain insights into the surface termination groups and to better understand the underlying mechanisms of the electrochemical etching process. **Figure 4.12** presents the XPS characterization results for porous 4H-SiC. Specifically, **Figure 4.12(a)** displays the survey spectra obtained from three randomly selected regions, while the corresponding atomic concentrations along with standard deviations are summarized in **Figure 4.12(b)**. High-resolution core-level spectra for key elements—Si, C, O, and F—are shown in **Figures 4.12(c) - (f)**, providing detailed chemical state information.

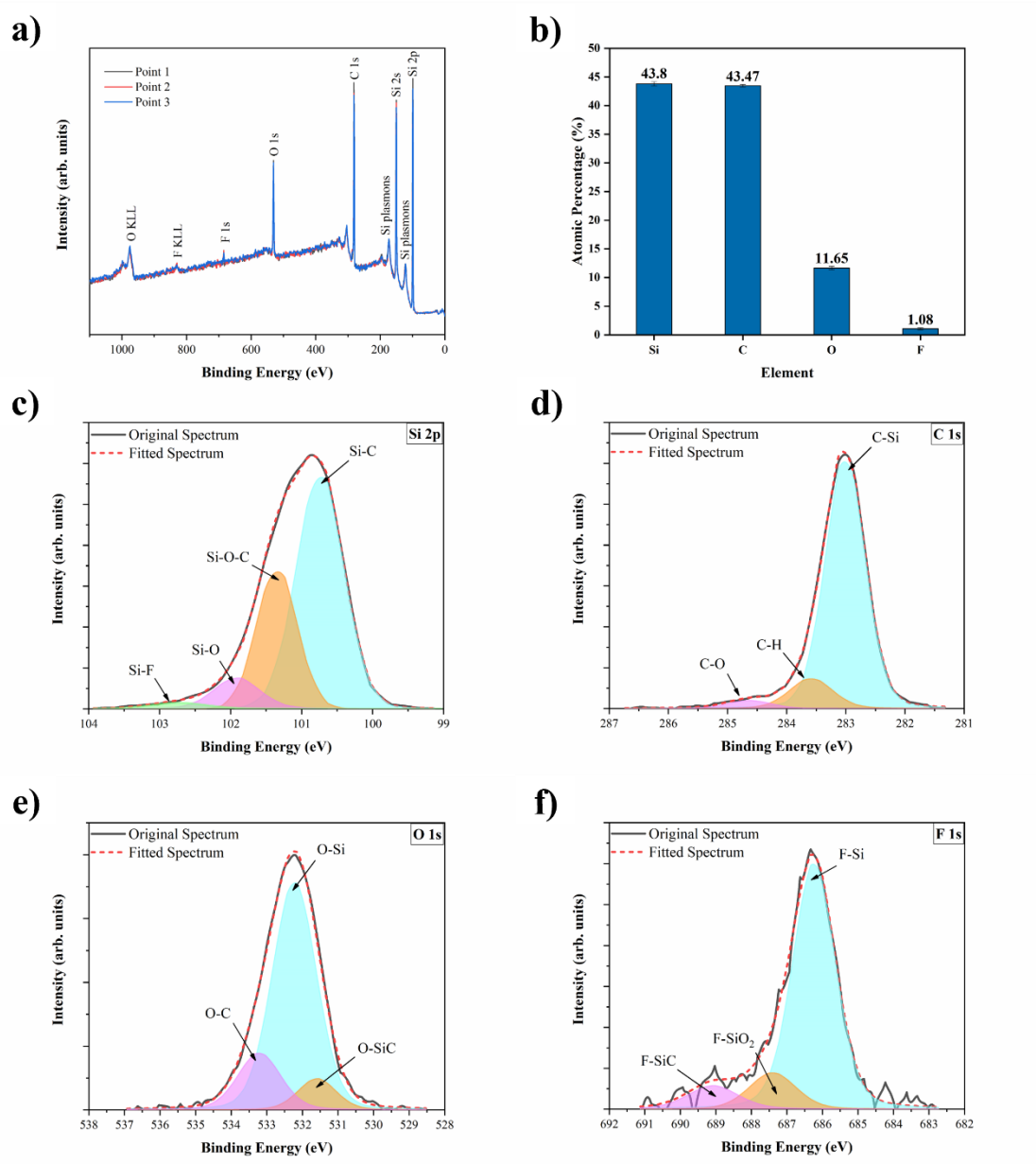

Figure 4. 12 XPS analysis of the white porous sample: (a) survey profile; (b) atomic percentage; core level spectra of (c) Si *2p*, (d) C *1s*, (e) O *1s*, and (f) F *1s* elements.**Error! Bookmark not defined.**

Based on the bonding conditions of each element, both the oxidation reaction and HF reaction can be verified by the existence of Si-O bonds and Si-F bonds. In the meantime, the detection of Si-O-C and F-SiO_2/SiC shows the incompletely oxidized

SiC and incompletely reacted SiO_2 separately, representing the intermediate states of these two reactions. (The details about the identification and analysis of peaks in each core level spectrum can be checked in this published paper[Error! Bookmark not defined.].) Combining the results of chemical bonds and the general chemical reactions of electrochemical etching, a more comprehensive mechanism (shown in **Figure 4.13**) was achieved to provide a more direct understanding. In general, the oxidation process breaks the Si-C bonds, and an O atom will be inserted to form Si-O-C bonds and transform into the typical crystal structure of SiO_2 gradually. The HF reaction will then substitute the Si-O bonds into Si-F bonds gradually. All the intermediate states can generate plenty of O-related and C-related defects, which may also affect the optical properties and will be discussed later.

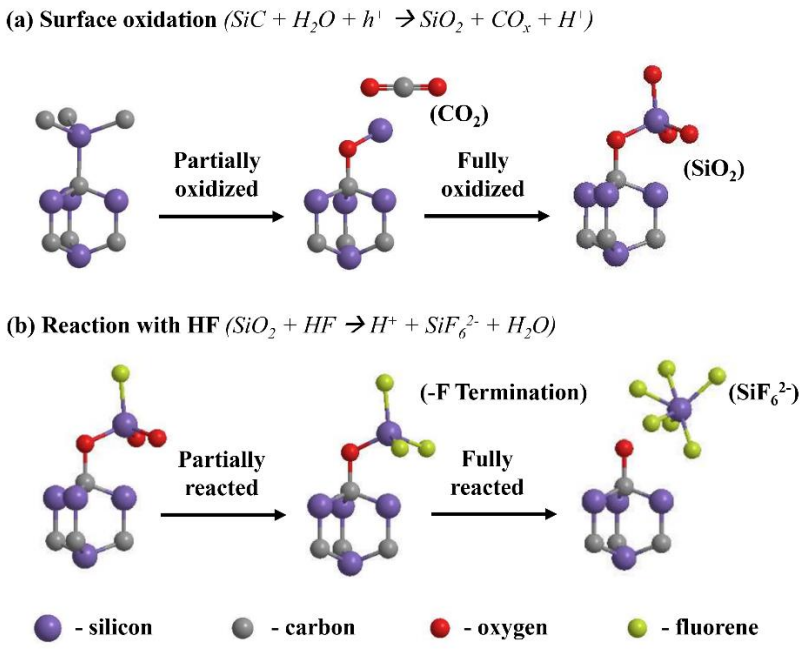

Figure 4. 13 Atomic model of electrochemical etching mechanism including (a) surface oxidation and (b) reaction with HF.[Error! Bookmark not defined.]

Size effects were also studied for this sample because quantum confinement effects play an important role in semiconductors. The comparison of Raman peaks is shown in **Figure 4.14(a)**, and there is a significant shift of the LO peak. This could be explained by the decrease in sizes (nano-needles observed by SEM), which affects both vibrational magnitudes and frequency of chemical bonds and directly determines the energy loss of elastic scattering based on the theory of Raman spectroscopy. The reduction of peak intensity is also reasonable due to the weaker incident light after strong reflections. Similarly, XRD spectrum can also help to study the size effect by using Scherrer equation[87] according to the broadening of peaks. As shown in **Figure 4.14(b)**, the white sample has an identical phase to the pristine wafer but also has broader peaks indicating the reduction of crystal size. Even though the quantitative calculation with Scherrer equation is very difficult for this sample because it requires the materials to have regular shapes (e.g., sphere) but our sample is much more complex with irregular needle-like structures, it is still consistent with Raman results showing their value in the study of size effects.

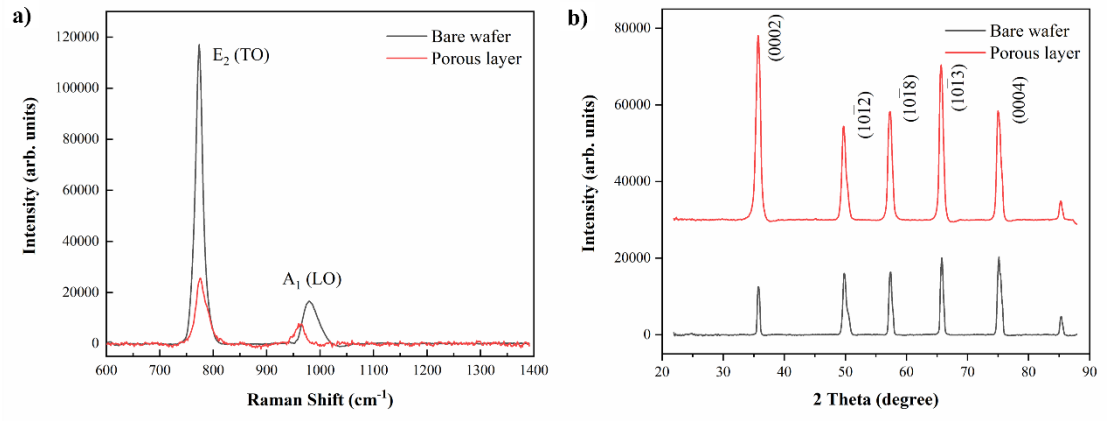

Figure 4. 14 (a) Raman spectrum and (b) XRD spectrum of the white sample compared with a pristine SiC wafer.**Error! Bookmark not defined.**

Furthermore, fluorescent properties are also measured to understand the effect of etching. As mentioned above in the reaction mechanism, the intermediate states of etching reactions produce many defects related to carbon, silicon, and oxygen, which are all regarded as surface defects and influence fluorescence. Based on both CL and PL measurements shown in **Figure 4.15**, the spectra change a lot compared to the pristine sample. Other than the band gap emission of 4H-SiC about 390 nm, the bought bare SiC wafers normally have another broad peak around 530 nm, which is commonly connected to C-related defects that might be generated during the manufacturing process[88]. However, after electrochemical etching, both the band-edge and C-related peaks are not observable, instead, an extremely broad peak appears, which could be explained by the formation of multiple types of defects such as O-related (~480 nm), C-related (~530 nm), and Si-related (~630 nm) peaks as deconvoluted[89]. The slight decrease in intensity could be also explained by the reflective surface similar to Raman

intensity, meanwhile, the low efficiency of defects related to non-radiative recombination may also be one of the reasons.

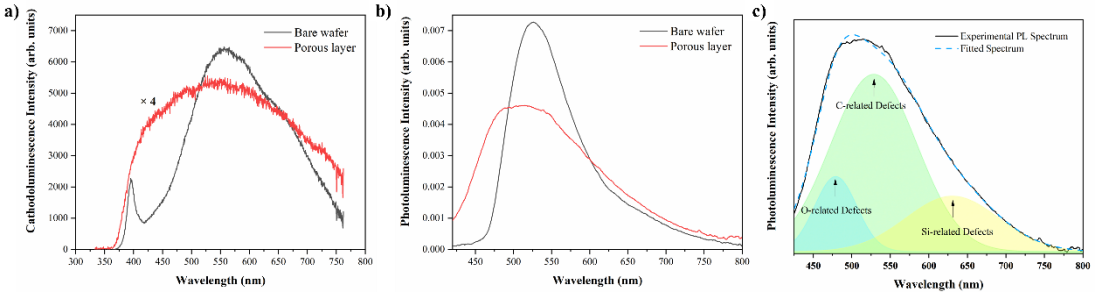

Figure 4. 15 Fluorescence properties of white porous sample: (a) CL and (b) PL spectra compared with the pristine SiC; (c) deconvolution of PL spectrum corresponding with certain types of defects.**Error! Bookmark not defined.**

4.4 Conclusion

In summary, electrochemical etching has been comprehensively studied on SiC semiconductor materials. The possibility of using new types of etchant (KOH) was explored with different parameters, while the key limitation is the low etching rate. Back to the most commonly used HF-based etching solution, all the key etching parameters have been explored with their effects on formed porous structures, and a formation mechanism combining oxidation and HF reaction rate has been proposed for future reference. Eventually, a special layered structure has been achieved with very high reflectivity (> 90%) for visible light by using a dilute HF solution, which shows a remarkable potential for the application of light reflectors. Besides, characterizations including surface chemistry, size effects, and fluorescence were also done to make a better understanding of the change of chemical bonds, formation of defects, and their

effects on optical properties.

Chapter 5

Effect of Defects on Electrochemical Etching

5.1 Introduction

During the etching process, it has been reported that a variety of defects can affect the etching such as dislocations and micropipes[90][91]. For conventional chemical etching, the existence of defects makes materials more sensitive to chemicals, thus a selectivity effect can be observed to inspect the presence of defects[92]. Recently, defects have also been created intentionally as a strategy to achieve selective etching for specific structures and devices. For instance, Jin et al. reported an approach to fabricating the Si nanotips by inducing defects by indentation and following with chemical etching[93]. Saito et al. achieved the selective formation of SiO_2 surface patterns assisted by chemical etching and micro-indentation[94]. Extending the indentation (points) to scratching (line), shows bigger potential to fabricate more complex patterns or structures. For example, Seo et al. also observed the selective etching effect on InP combined with surface scratching[95].

For the fabrication of SiC materials and devices, because of the difficulties coming from the ultra-high chemical stability of SiC as discussed above, it is very hard to use normal chemical etching methods as mentioned examples before. Wen et al. successfully achieved selective nanofabrication depending on the selective chemical

etching effects of defects induced by ion implantation[96]. According to their research, the mechanism is the amorphization and disordering effects given by ion-implantation makes SiC available to be etched chemically. However, it requires operating at an elevated temperature, and the etching rate is still very low. In the meantime, the ion implantation was operated by a focused-ion beam (FIB) system, which is well-known for characterizations combined with SEM but not suitable for large-scale production in industry. In this scenario, it still remains challenges for selective etching of SiC materials.

Therefore, in this chapter, we have conducted some research to explore the possibility of achieving selective etching based on electrochemical approaches. By inducing defects with surface scratching, it shows the protective effect on electrochemical etching and retains some micro-patterns after etching. The surface structures were comprehensively investigated based on multiple characterizations. Meanwhile, combining experimental evidence and simulation modeling, a mechanism is proposed to explain the selective etching behavior and study the influence factors on selectivity in the electrochemical etching process.

5.2 Experimental Details

The cleaned 4H-SiC dies were firstly scratched by using an Anton Paar Revetest Scratch Test machine with a diamond tip with a radius of 200 μm, where the scratching speed was kept at 4 mm/min and the value of applied force was adjusted. After surface

scratching, the samples were cleaned up again by deionized water and N_2 gas to remove the debris, and then went for electrochemical etching. The experiment process can be summarized in **Figure 5.1**. For the characterization methods, the surface morphology was directly observed through SEM and confocal microscopy, the surface topography was obtained by AFM, and the evidence of amorphization was proved by TEM. The simulation modeling was on COMSOL Multiphysics.

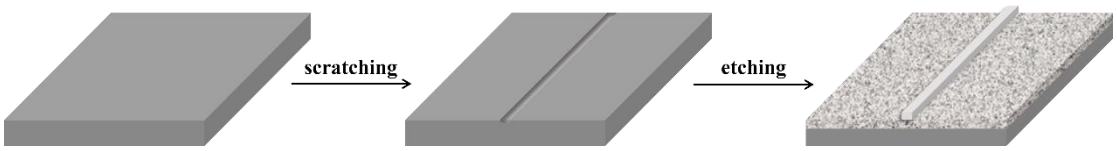

Figure 5. 1 Illustration of the experimental process.[97]

5.3 Results and Discussion

5.3.1 Characterizations of selectively etched surfaces

The surface morphologies of a scratched sample after etching are shown in **Figure 5.2**. Based on the SEM images, an interesting phenomenon can be observed the scratched line remains after electrochemical etching with a relatively smooth surface, while the surrounding region was just etched into a porous layer. This result shows that surface scratching can provide a protective effect during electrochemical etching, which is different from research about surface defects in conventional chemical etching with an enhanced etching effect.

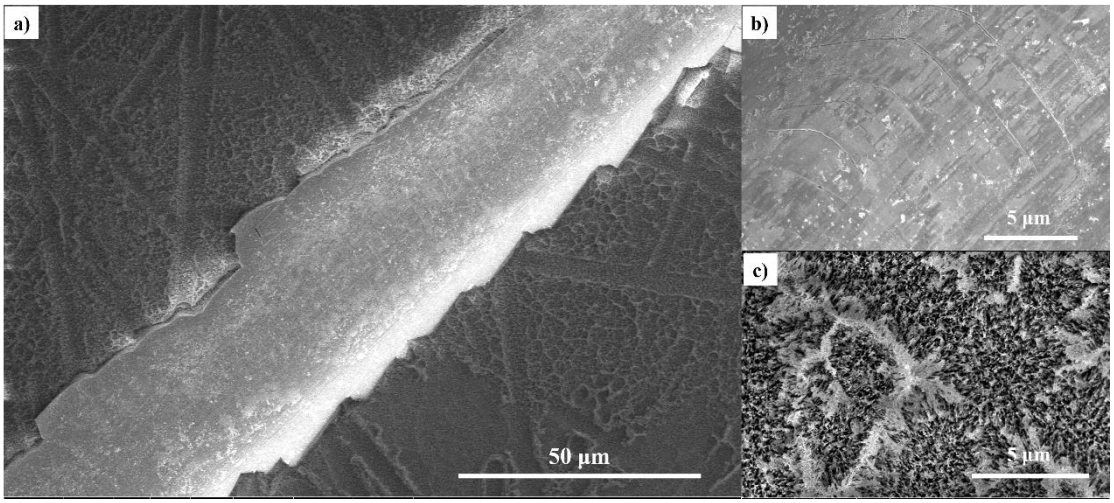

Figure 5. 2 SEM images of the scratched sample after electrochemical etching: (a) overall image; zoom-in images at (b) scratched pattern and (c) unscratched surface.**Error! Bookmark not defined.**

To obtain more details about the effect of surface scratching, the surface morphology after scratching but before etching was observed by applying a gradient of force from 1 to 30 N as shown in **Figure 5.3**. According to the image, a higher force tends to generate a wider scratch with larger and deeper defects. Because of the mechanical strength of SiC, lower forces make it hard to scratch the sample effectively. On the other hand, higher forces are more likely to generate many defects since SiC is brittle and will get deformed and fractured during the scratching process. Therefore, it is important to check the effects of forces on the final surface structures.

Figure 5. 3 Optical image of SiC surface scratched by a gradient force 1-30 N.**Error! B**

ookmark not defined.

Based on the previous observation, two typical values of forces were selected (8N and 24N) for further experiment and analysis. **Figure 5.4** exhibits confocal optical images showing the surface morphology after electrochemical etching. At the center of the images, the dark straight line is the formed pattern after etching. The surrounding greenish part is the etched porous region. The color represents the emission under 405 nm excitation, due to the generation of surface defects in porous structure based on the discussion in the previous chapters. The scratched patterns are much darker, which could be explained by the smaller number of defects since they have been protected during etching; or it is given by the height difference between scratched and un-scratched regions making them not in the same focusing plane.

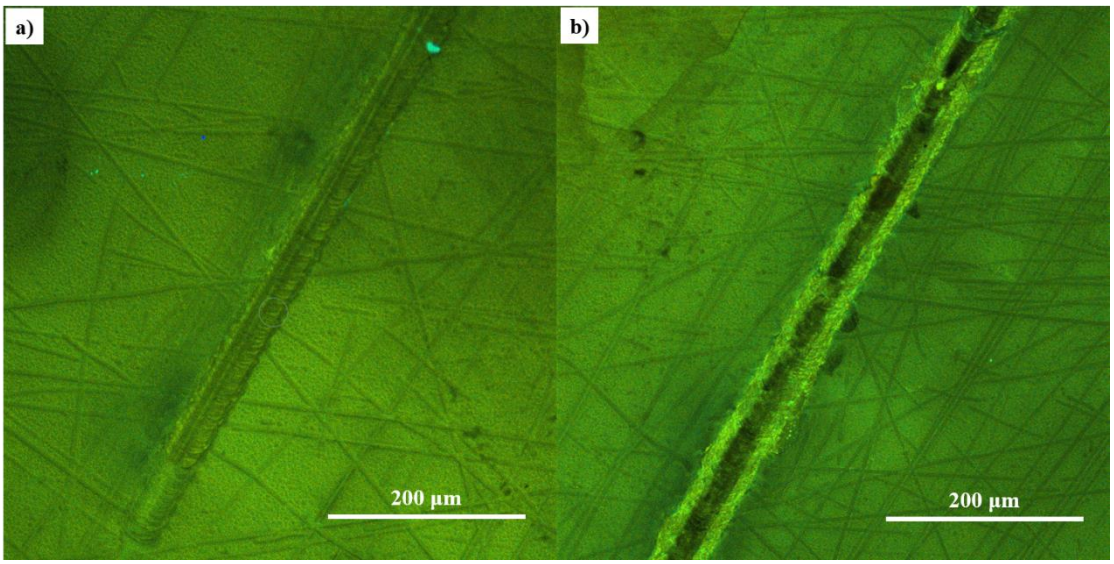

Figure 5. 4 Confocal optical images of sample scratched by (a) 8N and (b) 24N after electrochemical etching excited with 405 nm laser.**Error! Bookmark not defined.**

With the primary observation by microscopes, AFM was used to gain more information about surface morphologies. **Figure 5.5** includes the surface topography for the sample scratched by 8N. Comparing the surfaces before and after etching, the scratch-caused groove is transformed into a flat and smooth pattern. The width of the formed pattern is larger than the original groove but similar to the width of radio cracks, indicating the relationship between the scratched surface and the final pattern. From the depth profiles, the final pattern has a distinctive height difference compared to the nearby porous layer.

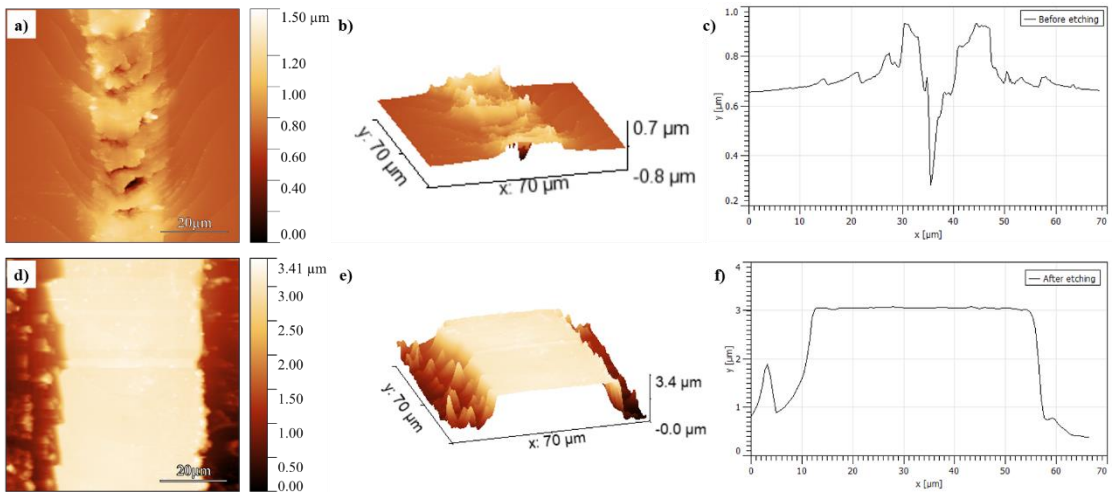

Figure 5. 5 AFM analysis for sample scratched with 8N including 2D images, 3D images, and depth profiles: (a)-(c) before etching, (d)-(e) after etching.**Error! Bookmark not defined.**

For sample scratched by 24N, it shows similar results as presented in **Figure 5.6**. With higher applied force, it creates deeper cracks and a larger groove before etching, consistent with our analysis by optical microscopy. After electrochemical etching, it still forms a pattern but has relatively poor surface flatness and smoothness. This surface

condition might be caused by more serious damage with higher applied force. Meanwhile, the higher value of force gives a wider pattern. Therefore, it should be optimized in fabrication to balance the width and surface perfections. In addition, the height of the achieved pattern for both samples is very similar, about 2.86 ± 0.21 μm (by 8N) and 2.93 ± 0.15 μm (by 24N), which suggests that height is independent of the value of forces. With the measured height difference between the porous region and the unetched region around 3.2 ± 0.02 μm, the etching rate can be calculated correspondingly, about 27 nm/min for the unscratched porous region and 2.5 nm/min for the scratched region.

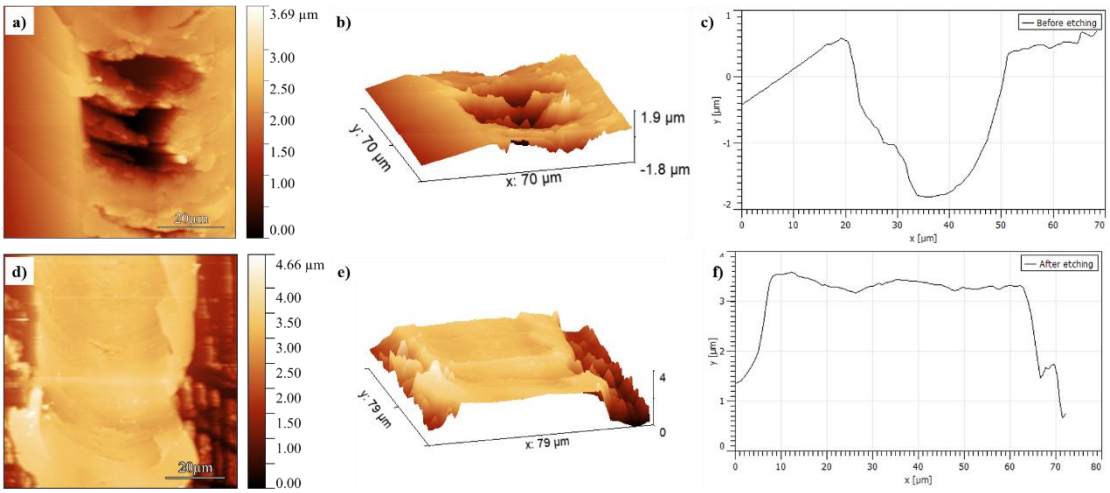

Figure 5. 6 AFM analysis for sample scratched with 24N including 2D images, 3D images, and depth profiles: (a)-(c) before etching, (d)-(e) after etching.**Error! Bookmark not defined.**

Now we have a better understanding of the surface morphology of samples after selective electrochemical etching, and the value of applied force is verified with relationships on the width of the formed pattern. However, there remains a question

about the mechanism. Based on the observation, there are some clues that the pattern aligns better with cracks or deformations instead of deep grooves. Further experiments should be conducted and will be discussed in the next section.

5.3.2 Study of selective etching mechanisms

To explore the mechanism of this selective etching phenomenon, it is important to refer to the basic reaction mechanisms of electrochemical etching. According to Chapter 4, there are two separate reactions including surface oxidation and HF reactions. From the previous section, we know that scratch plays a protective role on the surface during etching, therefore, it must have some influence on these two reactions. For chemical reactions, normally the surface defects will make the materials easier to be reacted or etched according to the literature review in the first part of this chapter. In this scenario, the accumulation of holes might be the key factor.

Based on the literature review, it has been confirmed that indentation or scratch can generate amorphization of SiC[98][99], and it is known that electric conductivity is always poorer than single crystals. Combined with the discussion in Chapter 4, the electric field affects the accumulation of holes on the surface and plays an essential role in the final surface structures. Therefore, speculation can be obtained that surface scratching could form amorphized regions of SiC and change the distribution of electric fields to prevent the holes from accumulating at the surface.

To verify the speculation, TEM was done to directly check the amorphization

effects as shown in **Figure 5.7**. Based on the diffraction pattern, the sample is semi-crystalline with some dots referring to single crystals and rings referring to amorphous phases, which directly proves the sample has been amorphized during surface scratching.

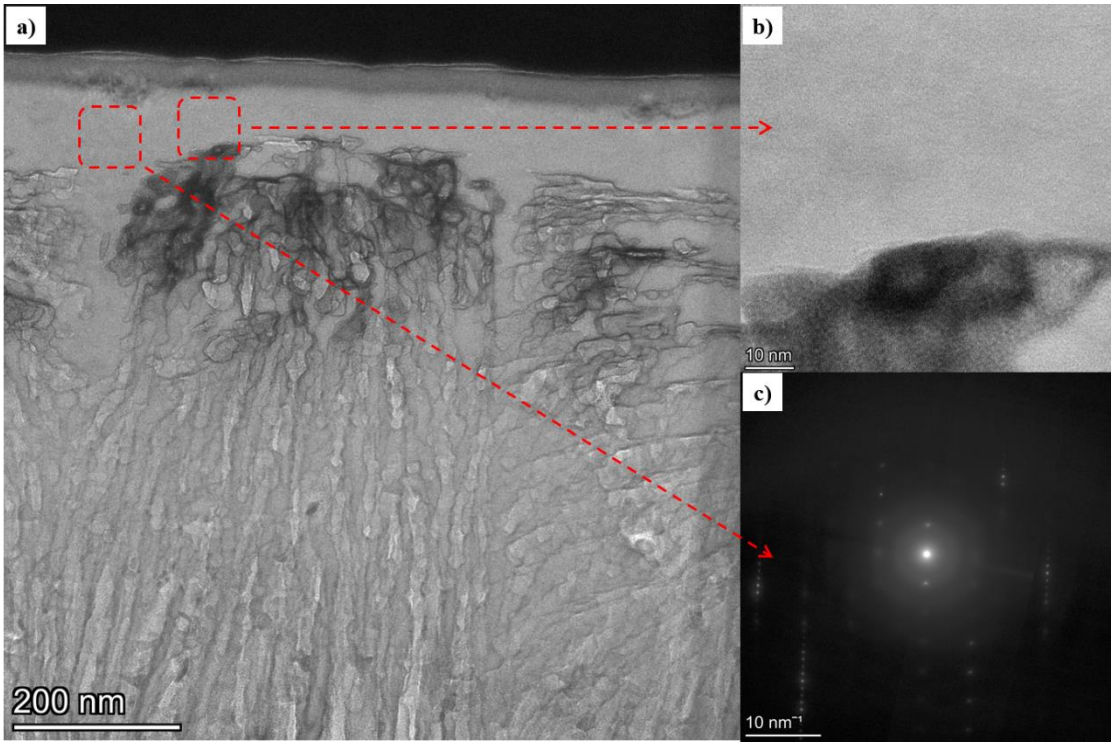

Figure 5. 7 TEM analysis of sample focused on the region underneath the surface with (a) overall image, (b) zoom-in image, and (c) diffraction pattern.**Error! Bookmark not defined.**

Apart from that, TEM-EDS analysis was also obtained at the same time to provide more information as shown in **Figure 5.8**. In particular, there is a lack of O and F signals on the top region near the surface, indicating that SiC does not appear to be oxidized and reacted by HF. This also helps to demonstrate that the surface of samples has been protected from oxidation reactions and is consistent with our speculation before.

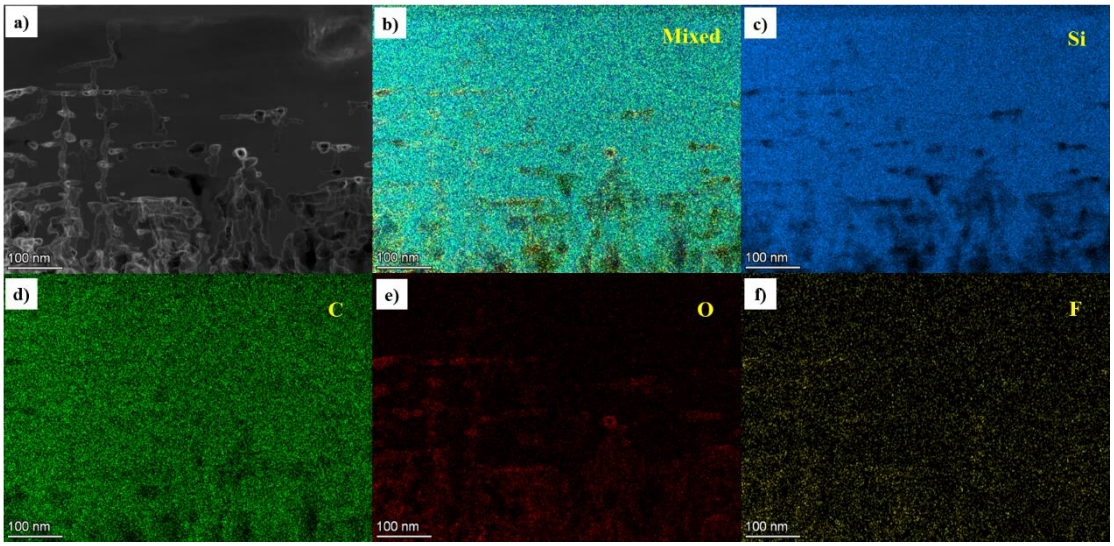

Figure 5. 8 TEM-EDS analysis including (a) overall image, (b) mixed elemental mapping image, and (c)-(f) elemental mapping results for Si, C, O and F separately.**Error! Bookmark not defined.**

Combining experimental observations, simulation modeling was also done to verify the idea of electric distribution visually. For the model shown in **Figure 5.9(a)**, a cuboid material was made, and on the top surface a semi-cylinder was set as an amorphized region, where the parameters were all followed by standard 4H-SiC and the only difference is their electric conductivity. Based on the simulation result shown in **Figure 5.9(b)**, there is a huge difference in current density between amorphized and surrounding regions. The value of electric conductivity is based on the literature review, where the amorphous SiC is in a range of 10^{-1} S/cm to 10^{-6} S/cm depending on the fabrication process [100][101]. In specific, the electric fields turn around the amorphized region, leading to an extremely low value of current density in the amorphous part. This result certifies the proposed mechanism that the change of electric field blocks the accumulation of holes and stops the surface oxidation reactions. Here

the difference in current density determines the etching selectivity.

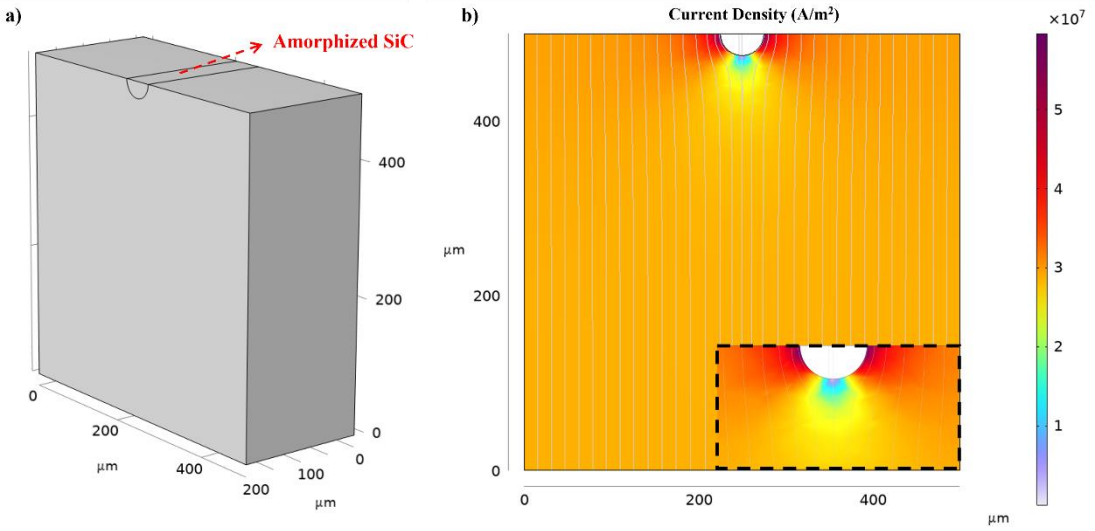

Figure 5. 9 (a) Constructed model; (b) simulated results exhibiting the electric field distribution and current density.**Error! Bookmark not defined.**

Due to the convenience of simulation, more studies were conducted to explore the effects of different factors on the etching selectivity. The first consideration is electric conductivity. Even though there remain questions about a precise relationship between surface scratching and the value of electric conductivity requiring further research, it can still be estimated that the degree of amorphization effect on single crystals could affect conductivity. To explore the influence of conductivity, a series of values of electric conductivity for the amorphous part were input. The etching selectivity is reflected by the ratio of current density, compared to the ratio of conductivity as demonstrated in **Figure 5.10(a)**. The result shows that the ratio of current density increases with the ratio of conductivity linearly, indicating that the etching selectivity is highly dependent on the value of conductivity. The other factor is about the size of the

amorphized region, since it has been shown that different forces could achieve a different scale of scratches. Similarly, by changing the size in the model and comparing the ratio of current density as exhibited in **Figure 5.10(b)**, it can be found that the etching selectivity does not affect too much by the size. In general, these simulations reveal that the change in electric conductivity plays the most important role in selective electrochemical etching.

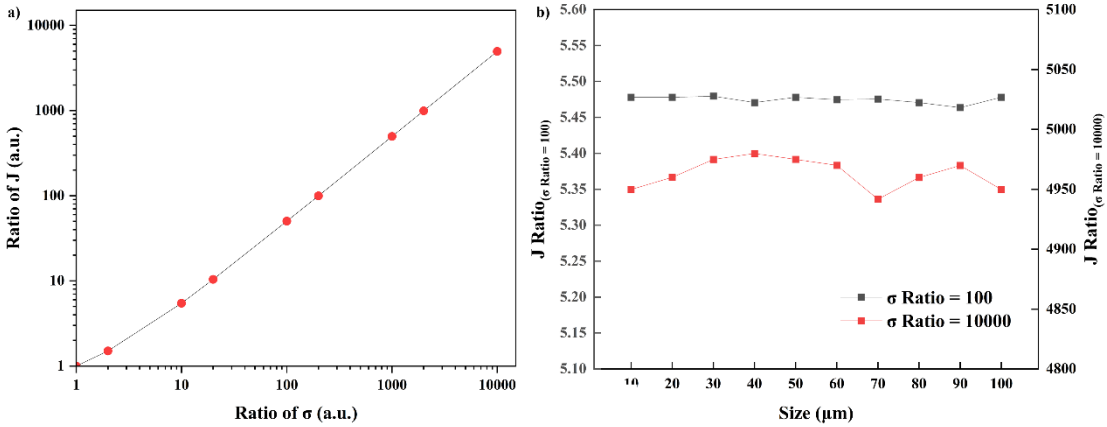

Figure 5. 10 Simulation study of the relationship (a) between the ratio of electric conductivity and current density; (b) between the size of the amorphized region and current density.**Error! Bookmark not defined.**

5.4 Conclusion

In this chapter, the effect of surface scratching on the electrochemical etching of SiC has been comprehensively studied and understood. The surface structures after etching have been observed and discussed, showing the possibility of using surface scratching to fabricate some patterns via electrochemical etching, where the influence of applied forces is analyzed. Furtherly, the selective etching mechanism has been successfully proposed and verified by both experiments and simulations, and concluded

as **Figure 5.11**. Such a selectivity effect on electrochemical etching is based on the electric field distribution and accumulation of holes, and the change of electric conductivity by amorphization is the key factor. More importantly, this finding broadens the possibilities and strategies for microfabrication combining the induced defects and electrochemical etching, and provides some suggestions for further research.

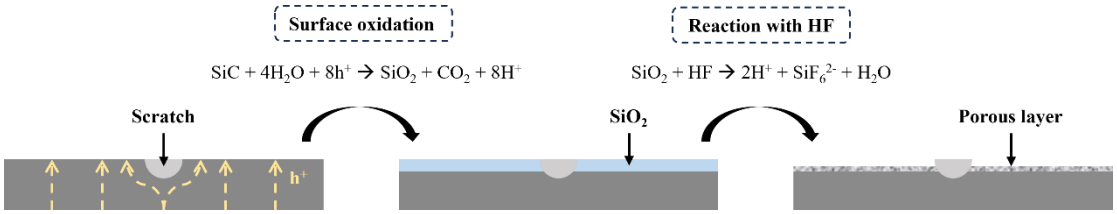

Figure 5. 11 Conclusion of mechanism of scratching-assisted electrochemical etching.**Error! Bookmark not defined.**

Chapter 6

Conclusions and Outlook

In this thesis, a comprehensive study of electrochemical etching strategy on SiC materials fabrication has been presented. A homemade electrochemical etching cell was manufactured based on the mechanisms and size of samples. The etching reaction mechanism was clarified with two separate steps: i) surface oxidation and ii) reaction with HF. The effects of different etching parameters such as etchant concentration and current density were explored for both KOH and HF aqueous solutions. KOH etchant in electrochemical solutions is a new attempt as a much safer alternation of HF, which successfully shows the availability of making porous SiC via electrochemical etching at room temperature. The KOH etching suffers from the problem of a low etching rate, which limits the application and requires further development in the future. For commonly used HF etchant, the influence of concentration and current density was verified corresponding to the chemical reactions, where current density mainly affects the first oxidation reaction by influencing the accumulation of holes, and the HF concentration affects the reaction rate of the second reaction. The formation of porous structures was explained by the localized electric field and accumulation of holes.

For the new findings and achievements, the highly reflective layered porous structures were achieved by electrochemical etching with a dilute HF solution and a

relatively high current density. The prepared sample was characterized by SEM and EDS to check the chemical composition and observe the surface morphology. Surface chemistry was analyzed by XPS to provide a better understanding of surface reaction and reconstruction. Size effects were also discussed by measuring Raman and XRD. The alternative thin layers of SiC and air structures have the multilayer interference effect, which provides a constructive enhancement of reflected light and causes high reflectivity. A simulation study was conducted to verify the idea and show a consistent result. Such a reflective structure not only extends the application of porous SiC as optical reflectors in high-temperature environments but also provides more possibilities for surface modification by electrochemical etching for optoelectronic applications.

Furthermore, the selective etching effects were achieved assisted by surface scratching, where the effects of defects on electrochemical etching were meticulously discussed. By characterizing the samples by optical microscopy, SEM, AFM and TEM, it has been shown that the surface scratch provides a protective effect and remains as micropatterns after etching, and the applied force during scratching can adjust the width of patterns. The formation mechanism was explained by the redistribution of electric fields caused by the change of electric conductivity of amorphized materials given by scratching. Combined with the simulation analysis, the lack of electric fields prevents the accumulation of holes on the surface and then blocks the surface oxidation reaction. This result provides a new simple strategy to fabricate SiC microstructures and devices, showing the potential to reduce the high cost of SiC dry etching.

As the requirements for sustainability and long-term development, earth abundant SiC must attract more attention and play more important roles in the future as one of the potential alternative materials in optoelectronics. In the future, precise control of etching parameters can be done to achieve more complex structures such as nanorods or nanowires. Additionally, amorphization of SiC can be achieved by other methods such as focused ion beams (FIB) or lasers, which could provide more accurate patterns or structures, and get closer to real applications.

Bibliography

[1] Neamen, Donald A., and Dhrubes Biswas. *Semiconductor physics and devices*. New York: McGraw-Hill higher education, 2011.

[2] Park, Taehyun, et al. "Overcoming downscaling limitations in organic semiconductors: Strategies and Progress." *Small* 20.9 (2024): 2306468.

[3] García de Arquer, F. Pelayo, et al. "Semiconductor quantum dots: Technological progress and future challenges." *Science* 373.6555 (2021): eaaz8541.

[4] De Leon, Nathalie P., et al. "Materials challenges and opportunities for quantum computing hardware." *Science* 372.6539 (2021): eabb2823.

[5] Awschalom, David D., and Michael E. Flatté. "Challenges for semiconductor spintronics." *Nature physics* 3.3 (2007): 153-159.

[6] Zhang, Shaohui, et al. "The rise of AI optoelectronic sensors: From nanomaterial synthesis, device design to practical application." *Materials Today Physics* 27 (2022): 100812.

[7] Kuroiwa, Yuichiro, Yu-ichiro Matsushita, and Fumiyasu Oba. "Unraveling crystal symmetry and strain effects on electronic band structures of SiC polytypes." *AIP Advances* 10.10 (2020).

[8] Goel, Saurav, and Anupam Agrawal. "Cutting hardness-an absolute measure after Mohs hardness Scale." *bdl* 2 (2013): 2Ft.

[9] Shi, Jueli, et al. "Wide bandgap oxide semiconductors: from materials physics to optoelectronic devices." *Advanced materials* 33.50 (2021): 2006230.

[10] Bolognesi, Alberto, et al. "Structural and Thermal Behavior of Poly (3-octylthiophene): a DSC, 13C MAS NMR, XRD, Photoluminescence, and Raman Scattering Study." *Macromolecular chemistry and physics* 202.12 (2001): 2586-2591.

[11] Shur, Michael, and Sergey L. Rumyantsev. *SiC materials and devices*. Vol. 1. world scientific, 2006.

[12] Kimoto, Tsunenobu, and James A. Cooper. *Fundamentals of silicon carbide technology: growth, characterization, devices and applications*. John Wiley & Sons, 2014.

[13] Tilley, Richard JD. *Defects in solids*. John Wiley & Sons, 2008.

[14] Ohtani, Noboru, et al. "Growth of large high-quality SiC single crystals." *Journal of crystal growth* 237 (2002): 1180-1186.

[15] Urakami, Yasushi, et al. "TSD Reduction by RAF (repeated a-face) Growth

Method." *Materials Science Forum*. Vol. 717. Trans Tech Publications Ltd, 2012.

[16] Kimoto, Tsunenobu. "Material science and device physics in SiC technology for high-voltage power devices." *Japanese Journal of Applied Physics* 54.4 (2015): 040103.

[17] Jiang, Liudi, and Rebecca Cheung. "A review of silicon carbide development in MEMS applications." *International Journal of Computational Materials Science and Surface Engineering* 2.3-4 (2009): 227-242.

[18] Zeng, Zheng, et al. "Changes and challenges of photovoltaic inverter with silicon carbide device." *Renewable and Sustainable Energy Reviews* 78 (2017): 624-639.

[19] Fedyanin, Dmitry Yu. "Optoelectronics of Color Centers in Diamond and Silicon Carbide: From Single-Photon Luminescence to Electrically Controlled Spin Qubits." Advanced Quantum Technologies 4.10 (2021): 2100048.

[20] Saddow, Stephen E. "Silicon carbide materials for biomedical applications." *Silicon carbide biotechnology*. Elsevier, 2016. 1-25.

[21] Knotter, D. Martin. "The chemistry of wet etching." *Handbook of cleaning in semiconductor manufacturing: fundamental and applications* (2010): 95-141.

[22] Zhuang, Dejin, and J. H. Edgar. "Wet etching of GaN, AlN, and SiC: a review." *Materials Science and Engineering: R: Reports* 48.1 (2005): 1-46.

[23] Vlaskina, S. I. "Silicon carbide LED." *Semiconductor Physics Quantum Electronics & Optoelectronics* (2002).

[24] Botsoa, J., et al. "Luminescence mechanisms in 6H-SiC nanocrystals." *Physical Review B—Condensed Matter and Materials Physics* 80.15 (2009): 155317.

[25] Ni, Zhenyi, et al. "Silicon nanocrystals: unfading silicon materials for optoelectronics." *Materials Science and Engineering: R: Reports* 138 (2019): 85-117.

[26] Yu, PeterY. *Fundamentals of semiconductors*. USA, 2005.

[27] Seo, Dong-Kyun, and Roald Hoffmann. "Direct and indirect band gap types in one-dimensional conjugated or stacked organic materials." *Theoretical Chemistry Accounts* 102.1 (1999): 23-32.

[28] Kitai, Adrian, ed. *Luminescent materials and applications*. John Wiley & Sons, 2008.

[29] Sakurai, Jun John, and Jim Napolitano. *Modern quantum mechanics*. Cambridge University Press, 2020.

[30] Segall, B., and G. D. Mahan. "Phonon-assisted recombination of free excitons in compound semiconductors." *Physical Review* 171.3 (1968): 935.

[31] Singh, Ashish Kumar, et al. "MATLAB user interface for simulation of silicon germanium solar cell." *Journal of Materials* 2015.1 (2015): 840718.

[32] Mokhov, Evgeniy N. "Doping of SiC crystals during sublimation growth and diffusion." *Crystal Growth*. IntechOpen, 2018.

[33] Troffer, T., et al. "Doping of SiC by implantation of boron and aluminum." *physica status solidi (a)* 162.1 (1997): 277-298.

[34] Monfort, Olivier, and Gustav Plesch. "Bismuth vanadate-based semiconductor photocatalysts: a short critical review on the efficiency and the mechanism of photodegradation of organic pollutants." *Environmental Science and Pollution Research* 25 (2018): 19362-19379.

[35] Shockley, William. "The Theory of p-n Junctions in Semiconductors and p-n Junction Transistors." *Bell system technical journal* 28.3 (1949): 435-489.

[36] Bera, Debasis, Lei Qian, and Paul H. Holloway. "Semiconducting quantum dots for bioimaging." *Drug Delivery Nanoparticles Formulation and Characterization*. CRC Press, 2016. 369-386.

[37] Vines, Lasse, Eduard Monakhov, and Andrej Kuznetsov. "Defects in semiconductors." *Journal of Applied Physics* 132.15 (2022).

[38] McCluskey, Matthew D., and S. J. Jokela. "Defects in zno." *Journal of Applied Physics* 106.7 (2009).

[39] Castelletto, Stefania, and Alberto Boretti. "Silicon carbide color centers for quantum applications." *Journal of Physics: Photonics* 2.2 (2020): 022001.

[40] Lebedev, A. A. "Deep level centers in silicon carbide: A review." *Semiconductors* 33 (1999): 107-130.

[41] Yan, Xiaolan, et al. "First-principles study of electronic and diffusion properties of intrinsic defects in 4H-SiC." *Journal of Applied Physics* 127.8 (2020).

[42] Turner, D. R. "On the mechanism of chemically etching germanium and silicon." *Journal of the electrochemical Society* 107.10 (1960): 810.

[43] Kadhim, Najah J., Stuart H. Laurie, and D. Mukherjee. "Chemical Etching of group III-V semiconductors." *Journal of chemical education* 75.7 (1998): 840.

[44] Ameta, Rakshit, et al. "Photocatalysis." *Advanced oxidation processes for waste water treatment*. Academic Press, 2018. 135-175.

[45] Gao, Chuanbo, Fenglei Lyu, and Yadong Yin. "Encapsulated metal nanoparticles for catalysis." *Chemical Reviews* 121.2 (2020): 834-881.

[46] Leonardi, Antonio Alessio, Maria José Lo Faro, and Alessia Irrera. "Silicon nanowires synthesis by metal-assisted chemical etching: A review." *Nanomaterials* 11.2 (2021): 383.

[47] Kong, Lingyu, et al. "Evidences for redox reaction driven charge transfer and mass transport in metal-assisted chemical etching of silicon." *Scientific reports* 6.1 (2016): 36582.

[48] Asoh, Hidetaka, Takayuki Yokoyama, and Sachiko Ono. "Formation of periodic microbump arrays by metal-assisted photodissolution of InP." *Japanese journal of applied physics* 49.4R (2010): 046505.

[49] Srivastava, Ravi P., and Dahl-Young Khang. "Structuring of Si into multiple scales by metal-assisted chemical etching." *Advanced Materials* 33.47 (2021): 2005932.

[50] Rysy, Stefan, Horst Sadowski, and Reinhard Helbig. "Electrochemical etching of silicon carbide." *Journal of Solid State Electrochemistry* 3 (1999): 437-445.

[51] Kuntyi, Orest, Galyna Zozulya, and Mariana Shepida. "Porous silicon formation by electrochemical etching." *Advances in Materials Science and Engineering* 2022.1 (2022): 1482877.

[52] Qasim, Mehdi, et al. "Radial Basis Function Neural Network Model for Optimizing Thermal Annealing Process Operating Condition." *Nano Hybrids* 4 (2013): 21-31.

[53] Bioud, Youcef A., et al. "Chemical composition of nanoporous layer formed by electrochemical etching of p-Type GaAs." *Nanoscale research letters* 11 (2016): 1-8.

[54] Kern, Werner. "Overview and evolution of silicon wafer cleaning technology." *Handbook of silicon wafer cleaning technology*. William Andrew Publishing, 2018. 3-85.

[55] Ji, Zimo, et al. "Highly reflective porous SiC with layered nanostructures formed by electrochemical etching." *Applied Surface Science* 694 (2025): 162797.

[56] *What Is Scanning Electron Microscopy? (How It Works, Applications ...* MSE Student, https://msestudent.com/what-is-scanning-electron-microscopy-how-it-works-applications-and-limitations/Accessed 15 May 2025.

[57] Nasir, Salisu, et al. "Potential Valorization of By-product Materials from Oil Palm: A review of Alternative and Sustainable Carbon Sources for Carbon-based Nanomaterials Synthesis." *BioResources* 14.1 (2019).

[58] Mulvaney, Shawn P., and Christine D. Keating. "Raman spectroscopy." *Analytical Chemistry* 72.12 (2000): 145-158.

[59] McNay, Graeme, et al. "Surface-enhanced Raman scattering (SERS) and surface-enhanced resonance Raman scattering (SERRS): a review of applications." *Applied spectroscopy* 65.8 (2011): 825-837.

[60] Chaichi, Ardalan, Alisha Prasad, and Manas Ranjan Gartia. "Raman spectroscopy and microscopy applications in cardiovascular diseases: from molecules to organs." *Biosensors* 8.4 (2018): 107.

[61] Teichert, Christian, and Igor Beinik. "Conductive atomic-force microscopy investigation of nanostructures in microelectronics." *Scanning Probe Microscopy in Nanoscience and Nanotechnology 2*. Berlin, Heidelberg: Springer Berlin Heidelberg, 2010. 691-721.

[62] Vandenbroucke, Arne. *Abatement of volatile organic compounds by combined use of non-thermal plasma and heterogeneous catalysis*. Diss. Ghent University, 2015.

[63] McNaught, Alan D. Compendium of chemical terminology. Vol. 1669. Oxford:

Blackwell Science, 1997.

[64] Martín, Francisco Ferrero, et al. "Optoelectronic instrumentation and measurement strategies for optical chemical (bio) sensing." *Applied Sciences* 11.17 (2021): 7849.

[65] Chazalviel, J-N., R. B. Wehrspohn, and F. Ozanam. "Electrochemical preparation of porous semiconductors: from phenomenology to understanding." *Materials Science and Engineering: B* 69 (2000): 1-10.

[66] Moshnikov, Vyacheslav A., et al. "Hierarchical nanostructured semiconductor porous materials for gas sensors." *Journal of non-crystalline solids* 356.37-40 (2010): 2020-2025.

[67] Kang, Jin-Ho, et al. "RGB arrays for micro-light-emitting diode applications using nanoporous GaN embedded with quantum dots." *ACS applied materials & interfaces* 12.27 (2020): 30890-30895.

[68] Hossain, S. M., et al. "Stability in photoluminescence of porous silicon." *Journal of luminescence* 91.3-4 (2000): 195-202.

[69] Chang, S-S., and R. E. Hummel. "Comparison of photoluminescence behavior of porous germanium and spark-processed Ge." *Journal of luminescence* 86.1 (2000): 33-38.

[70] Lee, Ki-Hwan, Seung-Koo Lee, and Ki-Seok Jeon. "Photoluminescent properties of silicon carbide and porous silicon carbide after annealing." *Applied Surface Science* 255.8 (2009): 4414-4420.

[71] Bourenane, K., et al. "Morphological and photoluminescence study of porous thin SiC layer grown onto silicon." *Surface and Interface Analysis: An International Journal devoted to the development and application of techniques for the analysis of surfaces, interfaces and thin films* 40.3-4 (2008): 763-768.

[72] Lu, Weifang, et al. "Temperature-dependent photoluminescence properties of porous fluorescent SiC." *Scientific reports* 9.1 (2019): 16333.

[73] Wang, Kaitao, et al. "High-performance ultraviolet photodetector based on single-crystal integrated self-supporting 4H-SiC nanohole arrays." *ACS Applied Materials & Interfaces* 15.19 (2023): 23457-23469.

[74] Rashid, Marzaini, et al. "Optical properties of mesoporous 4H-SiC prepared by anodic electrochemical etching." *Journal of Applied Physics* 120.19 (2016).

[75] Verhaverbeke, Steven, et al. "The etching mechanisms of SiO2 in hydrofluoric acid." *Journal of The Electrochemical Society* 141.10 (1994): 2852.

[76] Na, Moonkyong, et al. "Role of the oxidizing agent in the etching of 4H-SiC substrates with molten KOH." *Journal of the Korean Physical Society* 69 (2016): 1677-1682.

[77] Föll, Helmut, et al. "Formation and application of porous silicon." *Materials Science and Engineering: R: Reports* 39.4 (2002): 93-141.

[78] Naderi, N., and M. R. Hashim. "Effect of different current densities on optical properties of porous silicon carbide using photo-electrochemical etching." *Materials Letters* 88 (2012): 65-67.

[79] Rewatkar, Parwani M., et al. "Sturdy, monolithic SiC and Si3N4 aerogels from compressed polymer-cross-linked silica xerogel powders." *Chemistry of Materials* 30.5 (2018): 1635-1647.

[80] Wu, Suli, et al. "Reflection and transmission two-way structural colors." *Nanoscale* 12.21 (2020): 11460-11467.

[81] Wu, Renbing, et al. "Well-aligned SiC nanoneedle arrays for excellent field emitters." *Materials Letters* 91 (2013): 220-223.

[82] Chen, Shanliang, et al. "Highly flexible and robust N-doped SiC nanoneedle field emitters." *NPG Asia Materials* 7.1 (2015): e157-e157.

[83] Wang, Danyan, et al. "Structural color generation: from layered thin films to optical metasurfaces." *Nanophotonics* 12.6 (2023): 1019-1081.

[84] Palo, Emilia, and Konstantinos S. Daskalakis. "Prospects in broadening the application of planar solution-based distributed Bragg reflectors." *Advanced Materials Interfaces* 10.19 (2023): 2202206.

[85] Tan, Xiao, et al. "Anti-reflectance investigation of a micro-nano hybrid structure fabricated by dry/wet etching methods." *Scientific Reports* 8.1 (2018): 7863.

[86] Christidis, George, et al. "Broadband, high-temperature stable reflector for aerospace thermal radiation protection." *ACS applied materials & interfaces* 12.8 (2020): 9925-9934.

[87] Monshi, Ahmad, Mohammad Reza Foroughi, and Mohammad Reza Monshi. "Modified Scherrer equation to estimate more accurately nano-crystallite size using XRD." *World journal of nano science and engineering* 2.3 (2012): 154-160.

[88] Bawa, Salman, et al. "Porous SiC electroluminescence from p–i–n junction and a lateral carrier diffusion model." *Journal of Applied Physics* 129.4 (2021).

[89] Chen, Yun, et al. "Hybrid Anodic and Metal-Assisted Chemical Etching Method Enabling Fabrication of Silicon Carbide Nanowires." *Small* 15.7 (2019): 1803898.

[90] Weyher, J. L., et al. "Defect-selective etching of SiC." *physica status solidi (a)* 202.4 (2005): 578-583.

[91] Weyher, J. L. "Characterization of wide-band-gap semiconductors (GaN, SiC) by defect-selective etching and complementary methods." *Superlattices and microstructures* 40.4-6 (2006): 279-288.

[92] Tsuchida, H., I. Kamata, and M. Nagano. "Investigation of defect formation in 4H-SiC epitaxial growth by X-ray topography and defect selective etching." *Journal of Crystal Growth* 306.2 (2007): 254-261.

[93] Jin, Chenning, et al. "Site-controlled fabrication of silicon nanotips by indentation-induced selective etching." *Applied Surface Science* 425 (2017): 227-232.

[94] Saito, Yasuhiro, et al. "Fabrication of micro-structure on glass surface using micro-indentation and wet etching process." *Applied Surface Science* 254.22 (2008): 7243-7249.

[95] Seo, Masahiro, and Tadafumi Yamaya. "Selective formation of porous layer on n-type InP by anodic etching combined with scratching." *Electrochimica acta* 51.5 (2005): 787-794.

[96] Wen, Xiaolei, et al. "Helium Ion-Assisted Wet Etching of Silicon Carbide with Extremely Low Roughness for High-Quality Nanofabrication." *Small Methods* 8.5 (2024): 2301364.

[97] Ji, Zimo, et al. "Selective Formation of SiC Micropatterns by Scratching-patterned Electrochemical Etching." *Surfaces and Interfaces* (2025): 107285.

[98] Meng, Binbin, Yong Zhang, and Feihu Zhang. "Material removal mechanism of 6H-SiC studied by nano-scratching with Berkovich indenter." *Applied Physics A* 122 (2016): 1-9.

[99] Hu, Jiahao, et al. "On the deformation mechanism of SiC under nano-scratching: An experimental investigation." *Wear* 522 (2023): 204871.

[100] Zheng, Jia, et al. "Electrical and optical properties of amorphous silicon carbide thin films prepared by e-beam evaporation at room temperature." *Journal of Non-Crystalline Solids* 576 (2022): 121233.

[101] Gradmann, Rena, et al. "Si and SiC nanocrystals in an amorphous SiC matrix: Formation and electrical properties." *physica status solidi c* 8.3 (2011): 831-834.